

## McFACTS II: Mass Ratio–Effective Spin Relationship of Black Hole Mergers in the AGN Channel

HARRISON E. COOK <sup>1</sup>, BARRY MCKERNAN <sup>2,3,4,5</sup>, K.E. SAAVIK FORD <sup>2,3,4,5</sup>, VERA DELFAVERO <sup>6</sup>,  
KAILA NATHANIEL <sup>7</sup>, JAKE POSTIGLIONE <sup>3,5</sup>, SHAWN RAY <sup>5</sup>, AND RICHARD O’SHAUGHNESSY <sup>7</sup>

<sup>1</sup>New Mexico State University, Department of Astronomy, PO Box 30001 MSC 4500, Las Cruces, NM 88001, USA

<sup>2</sup>Center for Computational Astrophysics, Flatiron Institute, 162 5th Ave, New York, NY 10010, USA

<sup>3</sup>Department of Astrophysics, American Museum of Natural History, New York, NY 10024, USA

<sup>4</sup>Department of Science, BMCC, City University of New York, New York, NY 10007, USA

<sup>5</sup>Graduate Center, City University of New York, 365 5th Avenue, New York, NY 10016, USA

<sup>6</sup>Gravitational Astrophysics Laboratory, NASA Goddard Space Flight Center, Greenbelt, MD 20771, USA

<sup>7</sup>Center for Computational Relativity and Gravitation, Rochester Institute of Technology, Rochester, New York 14623, USA

### ABSTRACT

We use the Monte Carlo For AGN (active galactic nucleus) Channel Testing and Simulation (McFACTS<sup>a</sup>) code to study the effect of AGN disk and nuclear star cluster parameters on predicted mass distributions for LIGO-Virgo-KAGRA (LVK) compact binaries forming in AGN disks. The assumptions we vary include the black hole (BH) initial mass function, disk model, disk size, disk lifetime, and the prograde-to-retrograde fraction of newly formed black hole binaries. Broadly we find that dense, moderately short-lived AGN disks are preferred for producing a  $(q, \chi_{\text{eff}})$  anti-correlation like those identified from existing gravitational wave (GW) observations. Additionally, a BH initial mass function ( $\text{MF} \propto M^{-2}$ ) is preferred over a more top-heavy MF ( $M^{-1}$ ). The preferred fraction of prograde-to-retrograde is  $> 90\%$ , to produce results consistent with observations.

### 1. INTRODUCTION

Binary black hole (BBH) mergers are observed in gravitational waves (GW) at an increasing rate as LIGO-Virgo-KAGRA (LVK) improve detector sensitivities (e.g. The LIGO Scientific Collaboration et al. 2021, see also \*). Observed BBH include black holes with individual masses in the expected upper mass gap ( $\sim 50 - 120M_{\odot}$ ) where black holes are not expected from stellar evolution (Belczynski et al. 2016; Renzo & Smith 2024). A natural explanation for such black holes is hierarchical mergers in a dynamical environment, such as globular clusters (Rodriguez et al. 2018), nuclear star clusters (NSC) (Antonini & Rasio 2016) and active galactic nuclei (AGN) disks (McKernan et al. 2014; Bartos et al. 2017; Stone et al. 2017; Arca Sedda et al. 2023). Among hierarchical merger models, AGN are notable for both the efficiency of BBH formation as well as for retaining most post-merger products (as even strong kicks from mergers correspond to small orbital perturbations in such a deep potential well). BBH formation is driven through both the action of gas as a dynamical coolant and orbital migration producing rel-

atively low velocity dynamical encounters (e.g. Rowan et al. 2023; Qian et al. 2024; Dodici & Tremaine 2024). The result is a high rate of intermediate mass black hole (IMBH) formation relative to other channels (McKernan et al. 2012; Bellovary et al. 2016; Secunda et al. 2021; Yang et al. 2019; McKernan et al. 2020b; Tagawa et al. 2020b; Vaccaro et al. 2024). The rate of BBH mergers from AGN is also expected to be significantly higher than from quiescent NSCs (Ford & McKernan 2022).

The observed population of BBH mergers intrinsically favors positive effective spin (The LIGO Scientific Collaboration et al. 2021), implying formation channels bias spin directions towards alignment with BBH orbital angular momentum. This is not expected from gas-free hierarchical merger channels, but can occur in the AGN channel as black holes are torqued towards alignment with the gas disk over time (Tagawa et al. 2020a; Vajpeyi et al. 2022; McKernan & Ford 2024). Additionally, there is a possible anti-correlation observed in the  $(q, \chi_{\text{eff}})$  distribution of BBH mergers (Callister et al. 2021). This seems difficult to achieve in other merger channels but may be a relatively straightforward outcome in the AGN channel (McKernan et al. 2022a; Santini et al. 2023; Dittmann et al. 2024).

Here we present a study using the new McFACTS code (Monte Carlo For AGN Channel Testing and Simula-

<sup>a</sup>) <https://www.github.com/mcfacts/mcfacts>

\* <https://gracedb.ligo.org/superevents/public/O4/>

tions: McKernan et al. 2024, hereafter Paper I) to test the predictions of the AGN channel for the  $q - \chi_{\text{eff}}$  distribution across a wide range of parameter space in both AGN disk and NSC models, with a view to tightly constraining requirements on the AGN channel. (Delfavero et al. 2024, hereafter Paper III) presents the first study of the AGN channel in a semi-realistic Universe of AGN and NSCs.

This paper is organized as follows: We provide background information in Sect. 2 for the physical processes involved in our model. Sect. 3 describes the methods we use to vary model parameters. We report results in Sect. 4, discuss the possible implications in Sect. 5, and conclude in Sect. 6.

## 2. BACKGROUND

Gravitational wave observations provide information about each component mass and spin for a given BBH merger. In this work, we will focus on two specific BBH parameters: the binary mass ratio  $q = M_2/M_1$  ( $M_1 > M_2$ ), where  $M_1$  and  $M_2$  are the primary and secondary black hole masses; and effective spin of the BBH is given by

$$\chi_{\text{eff}} = \frac{M_1 \vec{\chi}_1 + M_2 \vec{\chi}_2}{M_1 + M_2} \cdot \hat{L}_{\text{bin}} \quad (1)$$

where  $\vec{\chi}_{1,2}$  are the dimensionless spin parameters associated with  $M_1, M_2$  respectively and  $\hat{L}_{\text{bin}}$  is the direction of the orbital angular momentum vector of the BBH.

For intuition in what follows, drawing spins ( $\vec{\chi}_{1,2}$ ) from a uniform distribution between aligned and anti-aligned with  $\hat{L}_{\text{bin}}$  means that the resulting  $\chi_{\text{eff}}$  distribution should be centered on  $\chi_{\text{eff}} \sim 0$ , with the width of that distribution a function of the initial spin magnitudes  $|\vec{\chi}_{1,2}|$ ; see, e.g., Callister (2021) for details. Within the AGN Channel, the range of  $q$  among first generation (1g; black holes produced via stellar evolution) mergers will depend on the range of the initial mass function (e.g. [10,40]  $M_{\odot}$ ) as well as the power-law of the mass distribution ( $\propto M^{-\gamma}$ ). A steeper mass function implies a bias towards  $q \sim 1$  as we are biased towards selecting similar mass black holes at the low mass end.

Conversely, a bias towards prograde BBH formation in the AGN channel would favor positive  $\chi_{\text{eff}}$  values in general. Such a bias might be due to orbital inclination flipping (Dittmann et al. 2024) of an inclined BBH, preferential ionization of retrograde BBH as they spend more time at wider separation (on average, Wang et al. 2021; Calcino et al. 2023), or some other mechanism. Additionally, once BBH merge, most of their orbital angular momentum as they coalesce will go into natal spin of the newly merged black holes, typically  $\chi \sim 0.7$  (Tichy & Marronetti 2008). Hierarchical mergers con-

taining higher generation (2g or higher) black holes that have inherited these large positive spins will therefore strongly favor positive  $\chi_{\text{eff}}$ .

## 3. METHODS

Here we introduce the assumptions, models, and parameters that we vary in the McFACTS code relevant for testing the  $q - \chi_{\text{eff}}$  distribution. For details of the code and further assumptions made therein see the discussion in Paper I. We run each setup 100 times to build a statistically significant sample.

### 3.1. Disk Models

As we cannot yet resolve them, the physical conditions of AGN disks are poorly constrained. Instead we rely on models fit to spectroscopic and multi-wavelength variability data. We use two common one-dimensional radial models Sirko & Goodman (2003, hereafter SG) and Thompson et al. (2005, hereafter TQM). In both cases we truncate the disk at some outer value  $R_{\text{out}}$ , assume the disk lives in a steady state for time  $\tau_{\text{AGN}}$ , and set an average disk aspect ratio of  $h = 0.03$ . Unless otherwise noted, disk models are constructed using the pAGN code (Gangardt et al. 2024a). Analogous to proto-planetary disks, migration traps may form between regions of outward and inward migration (Lyra et al. 2010). We include migration traps at 700  $R_g$  in SG disks and 500  $R_g$  in TQM disks (Bellovary et al. 2016).

### 3.2. Initial Black Hole Properties

We draw the initial black hole masses from a Pareto distribution with  $P(M) \propto M^{-\gamma}$ . We use  $\gamma = 2$  as the default throughout this paper and vary it to  $\gamma = 1$ . A steeper distribution (larger  $\gamma$ ) results in fewer high mass black holes initially, which we expect to reduce the number of unequal (low  $q$ ) mass mergers, whereas a shallower distribution will permit more low mass ratio encounters.

We draw the initial black hole spin directions  $\hat{\chi}$  from a uniform distribution over the interval  $[0, \pi]$  and the spin magnitudes from a Gaussian distribution centered at  $\mu_{\chi} = 0$  with standard deviation  $\sigma_{\chi} = 0.1$  as the default and test variations to  $\sigma_{\chi} = 0.02$  and 0.2. See Paper I for details on these models.

### 3.3. Disk Lifetimes

AGN lifetimes ( $\tau_{\text{AGN}}$ ) are thought to lie in the range  $\sim 0.1$  Myr to tens of Myr. The typical lifetime is hugely important, regulating how long each disk process operates to modify the nuclear system. We choose a default lifetime for SG disk models of  $\tau_{\text{AGN}} = 0.75$  Myr and

study variations of  $\tau_{\text{AGN}} = 0.5$  and 5 Myr. Since the TQM disk is generally less dense, we increase the default lifetime to  $\tau_{\text{AGN}} = 3$  Myr with variations of  $\tau_{\text{AGN}} = 2.5$  and 5 Myr.

### 3.4. Disk Size

The disk outer radius  $r_{\text{out}}$  determines what portion of the nuclear star cluster (NSC) will interact with the AGN disk; thus it dictates how many black holes will be embedded in the disk at the start of an AGN episode and how many NSC objects can be captured over the AGN disk lifetime. Our default disk size is  $5 \times 10^4 R_g$ , where  $R_g = GM/c^2$  is the gravitational radius (assuming a  $10^8 M_\odot$  SMBH – see below). We expect larger disk sizes that intersect with a larger portion of the NSC to produce more mergers, although this depends on the NSC radial density profile. Additionally, the initial pool of black holes also has greater distances through which to migrate and encounter possible companions that are unavailable in a smaller disk, possibly increasing the overall number of mergers. As such, since larger objects migrate faster, they encounter more objects, so we might expect larger disk sizes to drive lower  $q$  encounters.

### 3.5. Orbital Eccentricity

Gas drag acts to circularize orbits of eccentric prograde black holes over time. Once the orbital eccentricity is sufficiently small, migration and binary black hole formation become efficient. We draw initial eccentricities  $e_0$  from a uniform distribution between 0 and  $e_{0,\text{max}}$ . A relaxed (thermal) NSC has average eccentricity of  $e = 0.7$ . We choose fiducial values for the maximum in SG disks to be  $e_{0,\text{max}} = 0.5$  and in TQM disk to be  $e_{0,\text{max}} = 0.05$ , compensating for the lower density and longer circularization timescales. This choice assumes the NSC has insufficient time to fully relax between AGN disk episodes and that each such episode occurs in the same plane. We also explore setting  $e_0 = 0$  in the low density TQM model to bypass the long damping time.

### 3.6. Binary Formation

We form binaries from the circularized population when the separation between adjacent orbits reaches one Hill radius ( $R_H$ ) at the beginning of the time step, i.e.  $\Delta a = |a_1 - a_2| \leq 1R_H$ , where  $a$  is the semi-major axis,  $R_H = a_1 (M_1/3M_\bullet)^{1/3}$ ,  $M_1$  is the more massive candidate, and  $M_\bullet$  is the mass of the supermassive black hole. This choice contradicts recent two-dimensional hydrodynamical results showing binaries forming according to a chaotic mosaic of separations and drag conditions (Qian et al. 2024) that we intend to implement in future versions of the code.

### 3.7. Nuclear Star Cluster

Black holes with disk-crossing orbits will align to and become fully embedded in the disk over time (Fabj et al. 2020; Nasim et al. 2023; McKernan et al. 2022b; Wang et al. 2024). In each model, we draw these black holes from a nuclear star cluster with an outer radius of 5 pc and total mass  $M_{\text{NSC}} = 3 \times 10^7$ . The number of black holes to stars is  $N_{\text{BH}}/N_* = 10^{-3}$  according to Generozov et al. (2018) and the typical mass ratio is  $M_{\text{BH}}/M_* = 10^{-3}$ . The cluster is a “cored” type where the radial number density index changes at a critical radius  $R_{\text{crit}} = 0.25$  pc. When  $r < R_{\text{crit}}$ ,  $n \propto r^{-7/4}$  and  $n \propto r^{-2.5}$  elsewhere.

### 3.8. SMBH Mass

The mass of the central SMBH determines a variety of important disk conditions, including the density, scale height, and opacity profiles with radius. It also influences the NSC mass and outer disk radius. For this study we restricted ourselves to a single SMBH mass of  $10^8 M_\odot$ . We note that the standard TQM model uses an SMBH mass of  $10^9 M_\odot$ , but Paper III (Delfavero et al. 2024) finds  $\sim 10^8 M_\odot$  is likely to be the dominant contributor to AGN channel merger rates. In future studies we will produce a realistic distribution of SMBH and NSC masses, appropriate to our Universe, and consider the impact of those parameters on the  $q - \chi_{\text{eff}}$  relationship.

### 3.9. Retrograde Binary Fraction

We choose the binary angular momentum by drawing from a uniform distribution between 0 and 1 and control whether the binary forms prograde or retrograde depending on the number relative to the binary fraction  $f_{\text{ret}}$  we set. Binaries are expected to form with prograde orbital angular momenta, i.e., aligned with the disk orbital angular momentum ( $\vec{L}_{\text{bin}} \parallel \vec{L}_{\text{disk}}$ ), because retrograde binaries may experience extreme eccentricity pumping (Wang et al. 2021) or be flipped to prograde due to dynamical encounters (Samsing et al. 2022; McKernan & Ford 2024). For these reasons we choose  $f_{\text{ret}} = 0$  as our default, but we experiment with  $f_{\text{ret}} = 0.1$  and 0.5 to understand the impact of retrograde binaries on the  $q - \chi_{\text{eff}}$  space. Note, we do not allow for eccentricity pumping or dynamical flipping of retrograde binaries at this time.

### 3.10. Analysis Techniques

Understanding how efficiently various AGN systems produce high  $\chi_{\text{eff}}$  events is crucial for understanding the underlying fraction of AGN events contributing to the observed population and occurring in the Universe. We

separate merger events into three groups based on the generations of the black holes involved: (1) 1g mergers between first generation black holes (1g-1g), (2) 2g mergers involving second generation black holes (2g-1g and 2g-2g), and (3)  $\geq 3$ g mergers involving a third generation black hole or higher (3g-Ng). Sub-populations two and three are hierarchical mergers since they contain black holes produced via prior merger events.

Callister et al. (2021) report an anti-correlation between  $(q, \chi_{\text{eff}})$  with mean expectation values for the slopes of their “observed” and “predicted” samples of  $d\chi_{\text{eff}}/dq = -0.46$  and  $-0.49$ , respectively. We measure the influence of hierarchical mergers using a non-linear least squares fit to a line passing through the  $(q, \chi_{\text{eff}}) = (1, 0)$  and the hierarchical mergers. Shallower slopes (less negative) indicate a preference for larger  $q$  and lower  $\chi_{\text{eff}}$  or simply a lack of high  $\chi_{\text{eff}}$  mergers. Steeper slopes (more negative) can indicate a few possibilities: many large  $\chi_{\text{eff}}$  low  $q$  events, many large  $\chi_{\text{eff}}$  large  $q$  events, or both.

#### 4. RESULTS

Here we first explain the  $q - \chi_{\text{eff}}$  distribution of mergers from our fiducial models. Then, we demonstrate the effects of changing various input parameters on that  $q - \chi_{\text{eff}}$  parameter space.

##### 4.1. Reproducibility

Each panel in the figures produced for this paper can be reproduced using the correct seed. In the `Makefile`, change the `SEED` parameter to the value listed in Table 2. For random seeds using `Makefile`, add an empty line above `--seed`, comment out the `--seed` line and save the file. If a parameter needs to be changed, in each case, use the `model_choice_default.ini` file and change the appropriate parameter there.

##### 4.2. Default Models

The top left panel of Fig. 1 shows the mass ratio ( $q$ ) versus effective spin ( $\chi_{\text{eff}}$ ) (hereafter  $q - \chi_{\text{eff}}$ ) phase space for our default model consisting of 100 galaxies containing a SG disk with lifetime  $\tau_{\text{AGN}} = 0.75$  Myr, radius  $R_{\text{disk}} = 5 \times 10^4 R_g$ , and migration trap at  $700 R_g$ . We refer to this model as `sg_default`. The initial black hole population is drawn from a mass distribution of index  $\gamma = 2$  with a maximum initial orbital eccentricity  $e_{0,\text{max}} = 0.5$ . We only allow prograde orbiters to form binaries and do not allow the retrograde orbiters to interact in any way. We restrict binaries to form from black holes orbiting in a prograde orientation with the same sense of direction as the disk ( $\vec{L}_{\text{BH}} \parallel \vec{L}_{\text{disk}}$ ) and

**Table 1.** Unique parameters choices for each run. All other parameters are identical to those in the default models. The defaults are otherwise identical to those in Paper I (McKernan et al. 2024).

Run	Seed	Parameter	Value
<code>sg_default</code>	482821398	<code>disk_model_name</code>	<code>sirko-goodman</code>
		<code>timestep_num</code>	75
<code>tqm_default</code>	783822028	<code>disk_model_name</code>	<code>thompson_etal</code>
		<code>timestep_num</code>	300
		<code>disk_radius_trap</code>	500
		<code>disk_bh_orb_ecc_max_init</code>	0.05
<code>sg_g1</code>	40310999	<code>nsc_imf_powerlaw_index</code>	1
<code>tqm_g1</code>	63434937	<code>nsc_imf_powerlaw_index</code>	1
<code>sg_t0p5</code>	27228638	<code>timestep_num</code>	50
<code>sg_t5</code>	46249919	<code>timestep_num</code>	500
<code>tqm_t2p5</code>	75904298	<code>timestep_num</code>	250
<code>tqm_t5</code>	43913681	<code>timestep_num</code>	500
<code>sg_r2e4</code>	61693043	<code>disk_radius_outer</code>	$2e4$
<code>sg_r1e5</code>	80676180	<code>disk_radius_outer</code>	$10^5$
<code>tqm_r2e4</code>	37960990	<code>disk_radius_outer</code>	$2e4$
<code>tqm_r1e5</code>	64952404	<code>disk_radius_outer</code>	$10^5$
<code>sg_s0p02</code>	13555771	<code>nsc_bh_spin_dist_sigma</code>	0.02
<code>sg_s0p20</code>	33286099	<code>nsc_bh_spin_dist_sigma</code>	0.20
<code>tqm_s0p02</code>	74447390	<code>nsc_bh_spin_dist_sigma</code>	0.02
<code>tqm_s0p20</code>	10409162	<code>nsc_bh_spin_dist_sigma</code>	0.20
<code>sg_fr0p1</code>	38049133	<code>fraction_bin_retro</code>	0.1
<code>sg_fr0p5</code>	28559955	<code>fraction_bin_retro</code>	0.5
<code>tqm_fr0p1</code>	10171219	<code>fraction_bin_retro</code>	0.1
<code>tqm_fr0p5</code>	59253870	<code>fraction_bin_retro</code>	0.5
<code>sg_e0p1</code>	60447293	<code>disk_bh_orb_ecc_max_init</code>	0.1
<code>sg_e0p5</code>	33885262	<code>disk_bh_orb_ecc_max_init</code>	0.5
<code>sg_e0p7</code>	36123383	<code>disk_bh_orb_ecc_max_init</code>	0.7
<code>sg_e0p7_t1p5</code>	48962233	<code>disk_bh_orb_ecc_max_init</code>	0.7
		<code>timestep_num</code>	150
<code>tqm_e0p015</code>	85532667	<code>disk_bh_orb_ecc_max_init</code>	0.015
<code>tqm_e0p1</code>	20803120	<code>disk_bh_orb_ecc_max_init</code>	0.1
<code>tqm_e0_t1</code>	60471184	<code>disk_bh_orb_ecc_max_init</code>	0.0
		<code>timestep_num</code>	100
<code>tqm_e0</code>	92269440	<code>disk_bh_orb_ecc_max_init</code>	0.0

NOTE—The values for `disk_radius_trap` and `disk_radius_outer` are in units of gravitational radius  $R_g$ .

bias the resulting binaries towards a prograde direction (i.e.,  $\vec{L}_{\text{bin}} \parallel \vec{L}_{\text{disk}}$ , and see discussion of  $f_{\text{ret}}$  below). Retrograde single black hole orbiters do exist but are currently not allowed to form binaries or interact with the prograde population.

Gold points represent mergers where both black holes are first generation (1g-1g; hereafter 1g mergers). Inverted purple triangles are mergers with progenitor combinations of either 2g-1g or 2g-2g (hereafter 2g mergers). Red triangles indicate events with extreme hierarchical merger histories where at least one black hole is third generation or higher ( $\geq 3$ g-Ng; hereafter  $\geq 3$ g

mergers). The mean and standard deviation among the gold, purple, and red distributions, respectively, are  $(\bar{q}, \overline{\chi_{\text{eff}}}) = \{[0.69 \pm 0.21, -0.02 \pm 0.06], [0.54 \pm 0.21, 0.45 \pm 0.10], [0.34 \pm 0.18, 0.60 \pm 0.15]\}$  (see also Table 2).

The points lie in roughly two distributions: 1g mergers (gold circles) stay clustered around  $\chi_{\text{eff}} \sim 0$ , whereas 2g and  $\geq 3$ g (purple and red triangles, respectively) tend to have larger, positive  $\chi_{\text{eff}}$  values and trend towards smaller  $q$  values. Since  $10 M_{\odot}$  black holes are the most common from the IMF, then those in the 2g population will tend to be  $\sim 20 M_{\odot}$  leading to 2g-1g mergers concentrating around  $q \sim 0.5$ . Similarly, a given 3g-1g merger will typically concentrate at  $q \sim 1/3$ .

We quantify this anti-correlation between  $\chi_{\text{eff}}$  and  $q$  (larger  $\chi_{\text{eff}}$  values are measured for lower  $q$ ) using the slope of a line fit to the data and passing through  $(q, \chi_{\text{eff}}) = (1, 0)$ . In the top left panel of Fig. 1 the black solid line (fit to all points) has a slope of  $d\chi_{\text{eff}}/dq = -0.25 \pm 0.02$ . The gray dashed line is fit only to the hierarchical events ( $\geq 2$ g). The slope steepens to  $d\chi_{\text{eff}}/dq = -0.84 \pm 0.03$ , since hierarchical mergers tend to have larger  $\chi_{\text{eff}}$ . More negative slopes for the hierarchical population indicate a larger anti-correlation of  $\chi_{\text{eff}}$  with  $q$  and pulls the overall fit steeper as the fraction of hierarchical mergers increases.

The bottom left panel of Fig. 1 shows the results from our default TQM setup (`tqm_default`). All parameters are identical to those in the `sg_default` setup except the TQM disk model, a longer lifetime at  $\tau_{\text{AGN}} = 3$  Myr, and lower maximum initial orbital eccentricity  $e_{0,\text{max}} = 0.05$ . The 1g population is qualitatively similar as those occurring in the SG disk and concentrate around  $\chi_{\text{eff}} = 0$ , though spread over a wider range of  $\chi_{\text{eff}}$ , and the hierarchical mergers still shift towards positive  $\chi_{\text{eff}}$ , but only five 2g events and zero  $\geq 3$ g events occurred. The low density TQM disk produces drastically less mergers than a more dense SG disk despite a lifetime three times longer. Additionally, low disk opacity results in radiative feedback torques that dominate over inward migration torques causing a net outward migration for more massive objects that increases time between encounters.

The median mass ratio  $\bar{q} = 0.64 \pm 0.22$  for 1g mergers (gold points) for the TQM default is similar to the SG default. The spins are centered on zero but with larger standard deviation, such that  $\overline{\chi_{\text{eff}}} = -0.01 \pm -0.11$ . The wider spread in  $\chi_{\text{eff}}$  in TQM comes from a combination of (i) a lower surface density, leading to a longer damping time (allowing more eccentric 1g black holes to spin down to more negative  $\chi_{\text{eff}}$  for longer) as well as (ii) a longer overall disk lifetime (3 Myr) allowing more circularized 1g BH to spin up for longer.

The 2g sample (purple triangles) has a mean mass ratio of  $\bar{q} = 0.50 \pm 0.11$  and  $\overline{\chi_{\text{eff}}} = 0.52 \pm 0.10$ , though these statistics are for only five events. The paucity of hierarchical mergers results in an essentially flat  $d\chi_{\text{eff}}/dq = -0.02 \pm 0.03$  slope overall and an extreme  $d\chi_{\text{eff}}/dq = -1.01 \pm 0.07$  slope for the hierarchical sample.

Qualitatively, both plots tell us populations of higher generation mergers tend to have higher *positive*  $\chi_{\text{eff}}$ . This trend is reflected in  $\overline{\chi_{\text{eff}}}$  (see Table 2). Because we initialized the black hole spin orientations randomly, we expect  $\chi_{\text{eff}} \sim 0$  for 1g events. However, their remnants receive a natal spin of  $\chi \sim 0.7$  directed along the progenitor binary's angular momentum  $\vec{L}_{\text{bin}}$ . Since we limit binaries to form prograde,  $\vec{\chi}$  tends to point parallel to the disk angular momentum (positive). A black hole's mass and spin magnitude increase with generation, so we expect the hierarchical component of BBH mergers to be both more massive and have a higher spin, dominating Eq. (1) and leading low  $q$  events to have high  $\chi_{\text{eff}}$  values matching our findings (but see Sect. 4.7 for impacts of relaxing the strict prograde binary requirement to allow some fraction of binaries to form retrograde).

Below we explore the effects of a series of parameters on the intrinsic  $q - \chi_{\text{eff}}$  distributions produced by galaxies hosting a SG or TQM AGN disk model.

### 4.3. Changing the Mass Function

First, we test the effect of flattening the black hole initial mass function (IMF) by changing the power-law index from a steeper  $\gamma = 2$  (our default) to  $\gamma = 1$ . Nuclear star clusters (NSCs) may have a shallower-than-Salpeter IMF, and indeed a shallow IMF is observed in our own Galactic nucleus (Lu et al. 2013).

The top right panel of Fig. 1 shows the results from run `sg_g1` and is qualitatively similar to `sg_default`. We see the same population islands: a 1g merger population centered on  $\chi_{\text{eff}} \sim 0$ , as well as hierarchical populations at larger  $\chi_{\text{eff}}$ . However, given a shallower mass function or equivalently a harder IMF, the typical mass ratio shifts to smaller values, as expected. Thus, among the 1g-1g population we can see that the population is dispersed away from  $q \sim 1$ , evening out the slight tapering seen in the top left panel were  $\gamma = 2$ . From Table 2, among 1g mergers  $\bar{q}$  drops slightly from  $\bar{q} = 0.69 \pm 0.21$  from `sg_default` to  $\bar{q} = 0.66 \pm 0.21$  in `sg_g1`, while median  $\chi_{\text{eff}}$  remains the same. Among the higher generation mergers, visually there is a slight smearing out in both  $q, \chi_{\text{eff}}$  with the large  $q$  region filling in. Although  $\bar{q}, \overline{\chi_{\text{eff}}}$  remain similar to the default within the margins of error for both hierarchical populations,  $\geq 3$ g events have

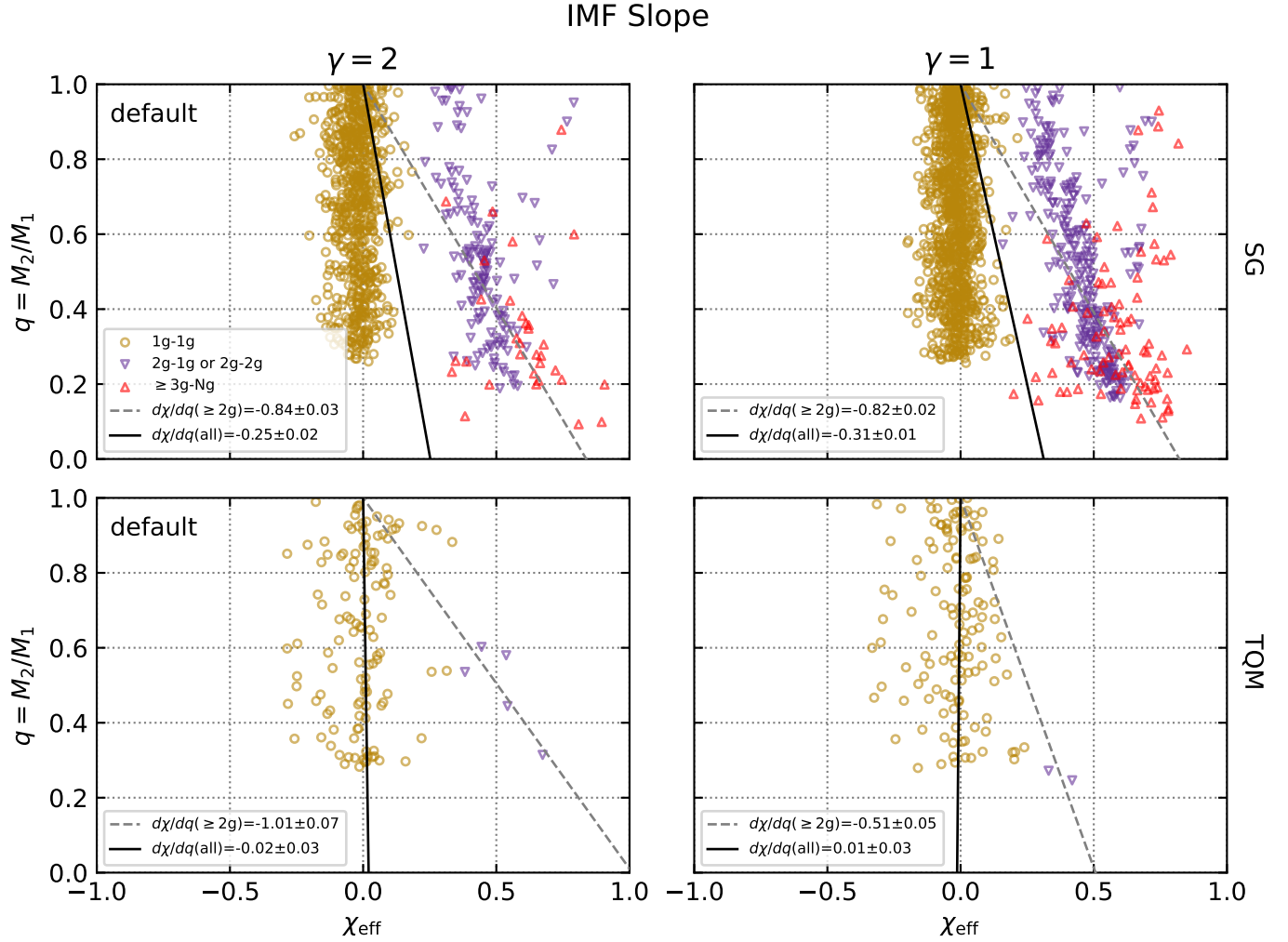


**Figure 1.** Mass ratio ( $q$ ) distribution as a function of  $\chi_{\text{eff}}$ . *Top left:* results from our default setup for a [Sirko & Goodman \(2003\)](#) disk with black hole mass distribution power-law index  $\gamma = 2$ , run `sg_default`. Gold points represent mergers where both black holes are first generation. Inverted purple triangles indicate mergers with progenitor combinations of either 2g-1g or 2g-2g. Red triangles indicate events with extreme hierarchical histories where at least one black hole is third generation or higher ( $\geq 3\text{g-Ng}$ ). The solid and dashed lines are fit through  $(\chi_{\text{eff}}, q) = (0, 1)$  and entire and  $\geq 2\text{g}$  populations, respectively. *Bottom left:* default setup for a [Thompson et al. \(2005\)](#) disk, run `tqm_default`. *Right column:* same as SG and TQM defaults but with shallower IMF index of  $\gamma = 1$  that increases the probability for high-mass black holes. Each experiment was performed for 100 galaxies. See [Table 1](#) for setup parameters and [Table 2](#) for population statistics.

median  $q$  smaller by more than 15% of their mean with more high  $\chi_{\text{eff}}$  - low  $q$  mergers occurring (see [Table 2](#)).

The slope of the overall fit measuring the anti-correlation decreases significantly from  $d\chi_{\text{eff}}/dq = -0.25 \pm 0.02$  to  $d\chi_{\text{eff}}/dq = -0.31 \pm 0.01$  with shallower IMF. The slope of the hierarchical mergers (those involving  $\geq 2\text{g}$  black holes) remains the same, subject to the uncertainties given by the standard deviation, so the change in overall slope seems mainly driven by the ability for more hierarchical mergers to form, given the larger Hill radius of heavier black holes, which increases the likelihood of binary formation.

As we flatten the black hole IMF from  $\gamma = 2$  in the `tqm_default` setup to  $\gamma = 1$  for setup `tqm_g1`, we do not see any visual difference comparing the two panels in the bottom row in [Fig. 1](#). The 1g population is statistically the same, and the 2g population shifts to lower mass ratio, but suffers from very small number statistics (two events). As for  $\gamma = 2$ , zero  $\geq 3\text{g}$  mergers occurred. The shift in the hierarchical line fit is, again, due to low number statistics, and the overall line fit does not significantly change.

For denser disks like SG, hierarchical mergers occur more readily as we flatten the mass function, since migration speed depends linearly on the mass (see [Paper I](#)).

The general increase in number of large  $\chi_{\text{eff}}$  hierarchical events of  $\geq 3g$  can most easily be seen in the steepening of the line fit to the overall population. Notably, no appreciable change occurs as a result of changing IMF slope in low density, low torque disks like TQM.

#### 4.4. Accretion Disk Lifetime

Next, we explore changes in the disk lifetime from our default models. We shorten the SG disk lifetime from  $\tau_{\text{AGN}} = 0.75$  Myr (default) to 0.5 Myr and increase it to 5 Myr. The TQM model has a longer default ( $\tau_{\text{AGN}} = 3$  Myr) which we decrease to 2.5 Myr and increase to 5 Myr. Fundamentally, the duration of accretion episodes limits how much time a black hole population has to evolve.

The top row of Fig. 2 shows the results for a SG disk with  $\tau_{\text{AGN}} = 0.5$  Myr (left, `sg_t0p5`) 0.75 Myr (center, `sg_default`), and 5 Myr (right, `sg_t5`). Decreasing the lifetime greatly decreases the number of 1g mergers, and there are now only a handful of 2g events, yet even these few events begin to trace the population islands seen previously and are found at statistically identical locations. Few black holes on eccentric orbits are able to circularize, migrate, form binaries, and merge in such a short disk lifetime. Increasing the lifetime also does not introduce statistically significant changes to populations, however the increased time allows  $\geq 3g$  mergers to fill in the low  $q$  and high  $\chi_{\text{eff}}$  (bottom right) corner of the space.

The bottom row of Fig. 2 shows the results for a TQM disk with  $\tau_{\text{AGN}} = 2.5$  Myr (left, `tqm_t2p5`) 3 Myr (center, `tqm_default`), and 5 Myr (right, `tqm_t5`). The 1g and 2g populations look very similar except for a slight shift towards lower  $\chi_{\text{eff}}$  for 1g mergers. This is likely caused by eccentric orbiter spinning down during circularization, but there are no statistically significant changes to any of the diagnostic quantities (see Table. 2).

In SG disks, lifetime does not have significant impact on the slopes of the hierarchical line fits but does decrease the uncertainty from  $d\chi_{\text{eff}}/dq = -0.83 \pm 0.06$  after 0.5 Myr to  $-0.84 \pm 0.03$  at 0.75 Myr to  $-0.83 \pm 0.02$  after 5 Myr. The overall line fit shows drastic change between 0.5 and 0.75 Myr, which shifts from  $-0.08 \pm 0.02$  at 0.5 Myr to  $-0.25 \pm 0.02$  at 0.75 Myr, but settles there at  $-0.34 \pm 0.01$  after 5 Myr. This overall steepening points to a correlation between the number of hierarchical mergers and disk lifetime, particularly in early times.

#### 4.5. Accretion Disk Radius

Next, we vary the radial extent of each disk model to  $2 \times 10^4$  and  $1 \times 10^5 R_g$  which affects the number of black holes initially in the disk. Fig. 3 shows the relevant results.

Smaller disks have a smaller cross section with the nuclear star cluster and will naturally result in a reduction in black hole mergers. This is reflected in the SG setup with  $R = 2 \times 10^4 R_g$  (top left, `sg_r2e4`). The number of mergers also decreases with larger disk size (top right, `sg_r1e5`). Although the number of black holes initially present in a larger disk increases, we populate the disk uniformly, so the distance between black holes in a disk with radius  $10^5 R_g$  is larger and thus encounters become less likely. The overall line fits for both radii are less than `sg_default` with the `sg_r2e4` disk producing  $d\chi_{\text{eff}}/dq = -0.27 \pm 0.04$  and the `sg_r1e5` disk producing  $d\chi_{\text{eff}}/dq = -0.08 \pm 0.05$ .

The already low number of mergers in the TQM disk goes to zero with a smaller disk radius (bottom left, `tqm_r2e4`). While the SG model saw a decrease in mergers for larger disks, the TQM model sees a slight increase in mergers for  $R = 10^5 R_g$  (bottom right, `tqm_r1e5`). This is because there is now more room for outwardly migrating black holes (the majority in this model) to encounter each other and overcome the increased separation. Additionally, the black holes spin up via mass accretion over longer migration distances which smears the 1g population to positive spin with  $\overline{\chi_{\text{eff}}} = 0.05 \pm 0.10$ . Also, `tqm_r1e5` is the first TQM setup to produce a non-zero slope in the overall line fit with  $d\chi_{\text{eff}}/dq = -0.15 \pm 0.02$ , but this is caused by the spin up of 1g mergers rather than a large hierarchical population as occurs in the SG runs.

Note: see Paper III for the effect on the merger rate for self-consistently changing outer disk radius with SMBH mass.

#### 4.6. Initial Black Hole Spin Magnitude Distribution

We explore the influence of the allowed spin magnitude distribution from which we make our draws during set up of the initial black hole population  $q - \chi_{\text{eff}}$ . We vary the width of the Gaussian distribution from  $\sigma = 0.1$  down to 0.02 and up to 0.2. In effect, this parameter controls how aligned the nuclear star cluster objects' spins are before the accretion disk forms.

In Fig. 4 we see each test produces the usual population islands as the default setups. For SG disks, no significant change occurs in  $\bar{q}$  for any of the generational subpopulations (top left: `sg_s0p02` and top right: `sg_s0p20`). However, we see the spread in  $\chi_{\text{eff}}$  1g population is greatly impacted and grows as the spin width increases from  $\sigma_\chi = 0.02$  to 0.20. The standard deviation on  $\overline{\chi_{\text{eff}}}$  reflects this trend, tightening to  $-0.01 \pm 0.02$  when  $\sigma_\chi = 0.02$  and broadening to  $-0.03 \pm 0.10$  when  $\sigma_\chi = 0.20$ . While no statistically significant change is seen in  $\overline{\chi_{\text{eff}}}$  or  $d\chi_{\text{eff}}/dq$  for the hierarchical populations

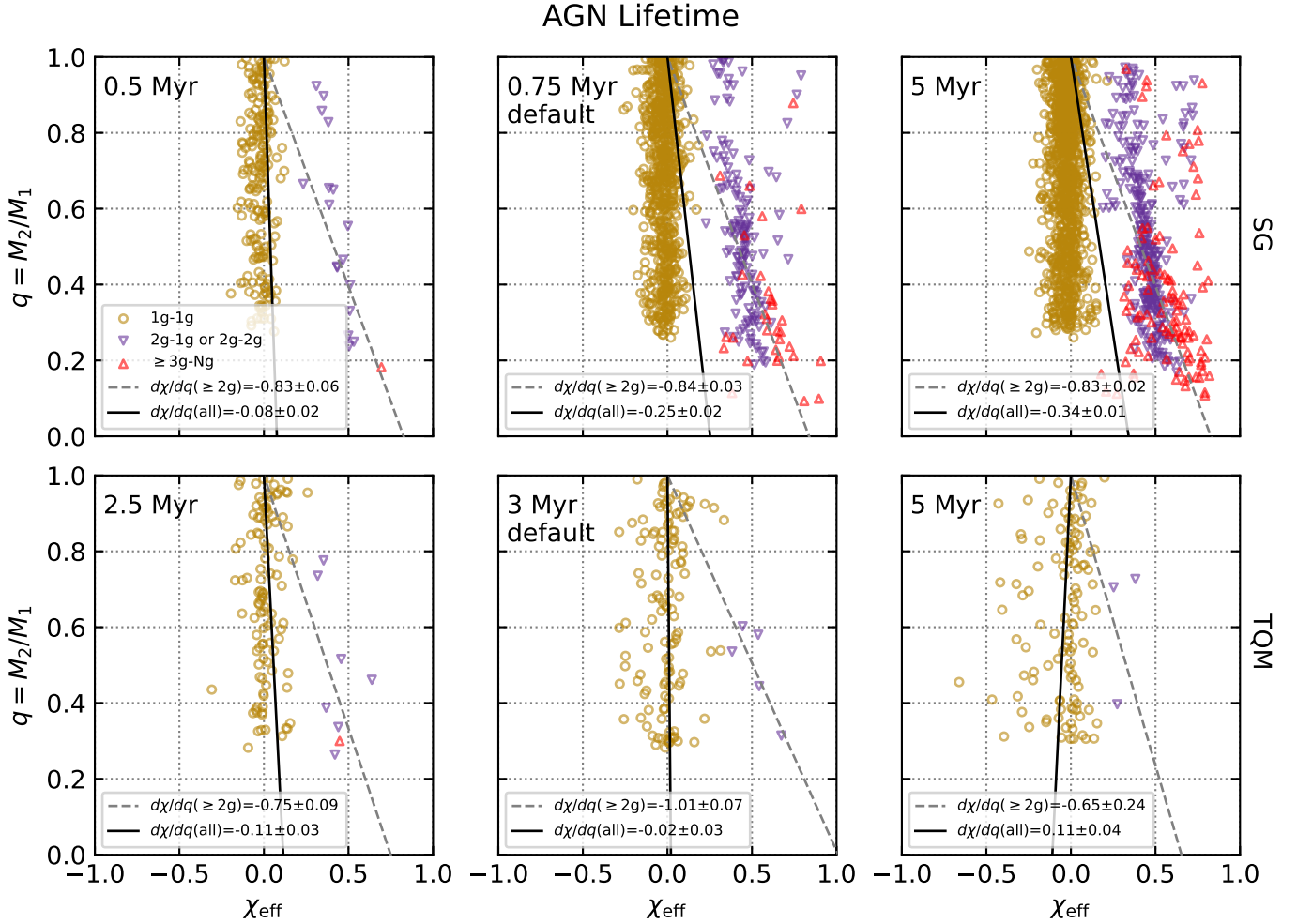


**Figure 2. Varying the disk lifetime.** *Top row:* SG disk setups with  $\tau_{\text{AGN}} = 0.5, 0.75,$  and  $5$  Myr. *Bottom row:* TQM disk setups with  $\tau_{\text{AGN}} = 2.5, 3,$  and  $5$  Myr. Slopes of lines fit to the overall population steepen with lifetime in dense SG disks as more hierarchical mergers with large  $\chi_{\text{eff}}$  occur, but lifetime has little impact on low density TQM disks. Markers are as in Fig. 1. See Table 1 for unique setup parameters and Table 2 for population statistics.

(since we anchored the line to  $\chi_{\text{eff}} = 0$ ), tighter initial distributions of spin magnitude cause hierarchical mergers to follow a tighter trend, whereas a wider distribution increases the scatter.

The TQM model shows similar behavior as the SG disk when varying the width of the initial spin magnitude distribution (bottom left: `tqm_s0p02` and bottom right: `tqm_s0p20`). The mean  $\bar{q}$  of 1g mergers stays the same, but the variance on  $\overline{\chi_{\text{eff}}}$  is correlated with increasing spin magnitude width. For  $\sigma_\chi = 0.02, 0.10, 0.20$ ,  $\overline{\chi_{\text{eff}}} = 0.01 \pm 0.0, -0.01 \pm 0.11, 0.03 \pm 0.13$ , respectively. The numbers of hierarchical mergers are too low to make any robust claims regarding their statistics.

If the detected population has a component with a wide distribution of  $\chi_{\text{eff}}$  centered around  $\chi_{\text{eff}} = 0$ , for the AGN channel this implies 1g black holes in NSCs have a broad range of initial spin values, possibly reflecting details of star formation and/or gas accretion

in the galactic nucleus. If the measured effective spins follow narrow distributions (both centered on  $\chi_{\text{eff}} \sim 0$  and at higher  $\chi_{\text{eff}}$ ), then 1g black holes in NSCs are likely born with a very narrow range of spins (close to zero). Constraints from future BBH catalogs (O4 and O5) on the width of the  $\chi_{\text{eff}}$  distribution will allow us to test models of star formation and black hole evolution in galactic nuclei.

Changing the width of the initial spin magnitude distribution does not appear to significantly impact the expectation values for either disk model. But the intrinsic distributions in spin are likely  $\sigma_\chi \leq 0.2$  in SG models since the standard deviation on  $\chi_{\text{eff}}$  for the 1g population resulting from this setting extends to negative  $\chi_{\text{eff}}$  about as far as Callister et al. (2021) report is observed. TQM models produce similar results for 1g mergers, but the number of hierarchical events remains limited.

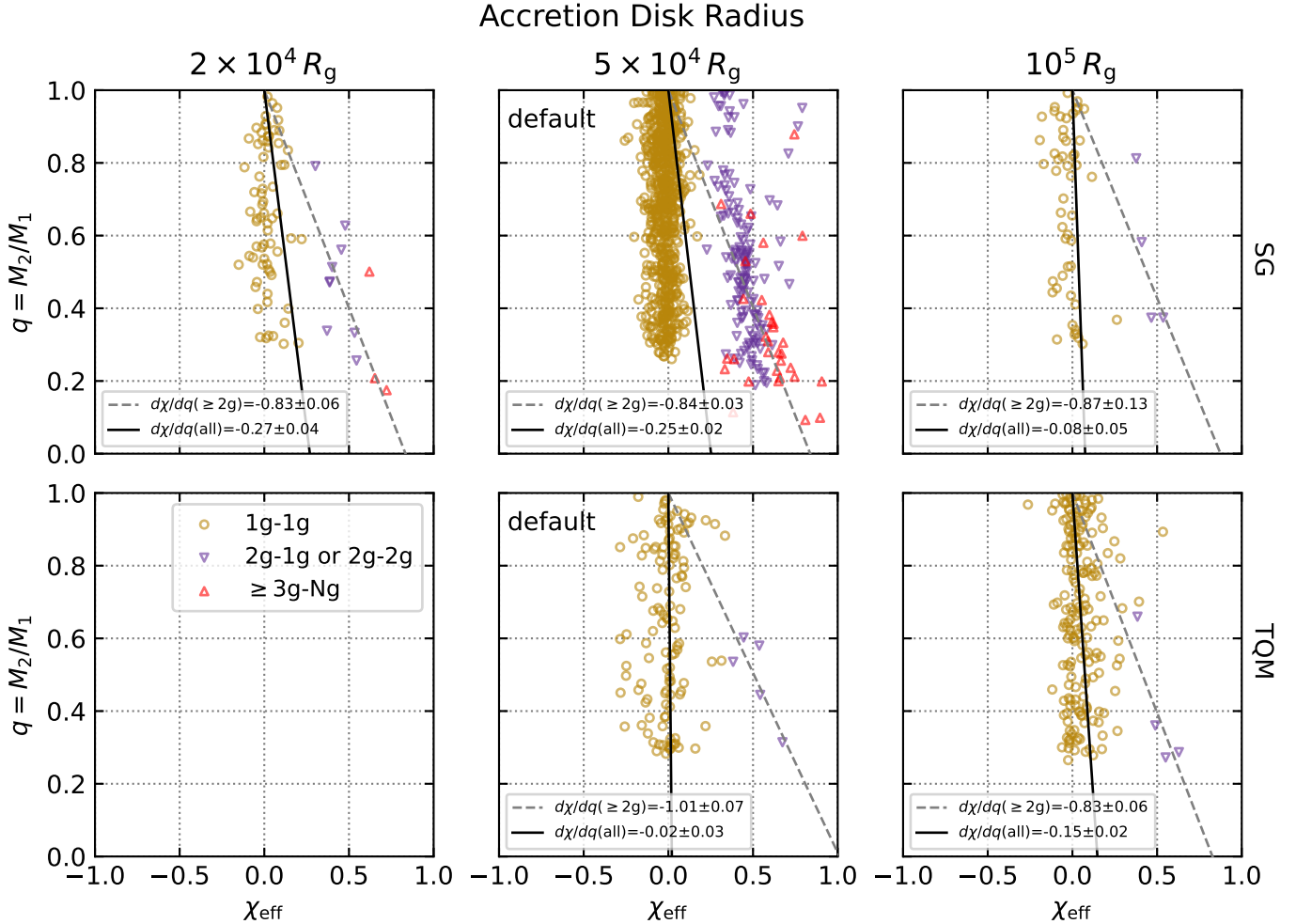


**Figure 3. Varying disk radius.** SG and TQM disks with radii  $r = (2 \times 10^4, 5 \times 10^4, 10^5) R_g$ . Both decreases and increases in disk radius result in fewer mergers. Markers are as in Fig. 1. See Table 1 for unique setup parameters and Table 2 for population statistics.

#### 4.7. Impact of Retrograde Binaries

We now relax the strict requirement for prograde binaries and allow the retrograde fraction  $f_{\text{ret}}$  to be 0.1 and 0.5. As a reminder, retrograde binaries have orbital angular momentum vectors pointing in the opposite direction of the angular momentum vector for their mutual orbit around the SMBH in the same direction as the disk and is taken to be positive. This happens when the black hole spins  $\vec{\chi}_{1,2}$  are anti-aligned with  $\vec{L}_{\text{bin}}$  or,  $\vec{\chi}_{1,2} \cdot \vec{L}_{\text{bin}} = -1$ .

The top row of Fig. 5 shows the results for increasing retrograde binary fraction in a SG disk. In each case, the 1g population remains symmetric about  $\chi_{\text{eff}} = 0$  without change from the fiducial setup. Allowing binaries to form retrograde primarily affects the hierarchical mergers, and we see a handful of these appear on the left side of the plot for  $f_{\text{ret}} = 0.1$ . When  $\vec{L}_{\text{bin}} < 0$  and  $\chi_{1,2} > 0$  for both black holes,  $\chi_{\text{eff}}$  will be negative. This

is also true when  $q$  is sufficiently small and the more massive black hole’s spin is pointed opposite to  $\vec{L}_{\text{bin}}$ . Increasing the retrograde fraction from  $f_{\text{ret}} = 0$  (top left, `sg_default`) to 0.1 (top center, `sg_fr0p1`), primarily affects the mean effective spin of the hierarchical population. For all hierarchical mergers,  $\overline{\chi_{\text{eff}}}$  decreases with increasing retrograde fraction as more negative  $\chi_{\text{eff}}$  events occur, but the standard deviation increases drastically as a result. For  $f_{\text{ret}} = 0$ ,  $\overline{\chi_{\text{eff}}} = 0.45 \pm 0.10$ , but when  $f_{\text{ret}} = 0.1$ ,  $\overline{\chi_{\text{eff}}} = 0.38 \pm 0.28$ . The  $\geq 3g$  population sees even greater uncertainty increases with  $\overline{\chi_{\text{eff}}} = 0.60 \pm 0.15$  changing to  $0.38 \pm 0.48$ .

The line fit slopes reflect these shifts towards negative  $\chi_{\text{eff}}$  with the hierarchical mergers’ slope shifting from  $d\chi_{\text{eff}}/dq = -0.84 \pm 0.03$  ( $f_{\text{ret}} = 0$ ) to  $-0.61 \pm 0.05$  ( $f_{\text{ret}} = 0.1$ ). This drastically impacts the overall fit’s slope as well, flattening from  $-0.25 \pm 0.02$  to  $-0.21 \pm 0.02$ . Even a few negative  $\chi_{\text{eff}}$  hierarchical events when will skew the measurement.

## Width of IMF Spin Distribution

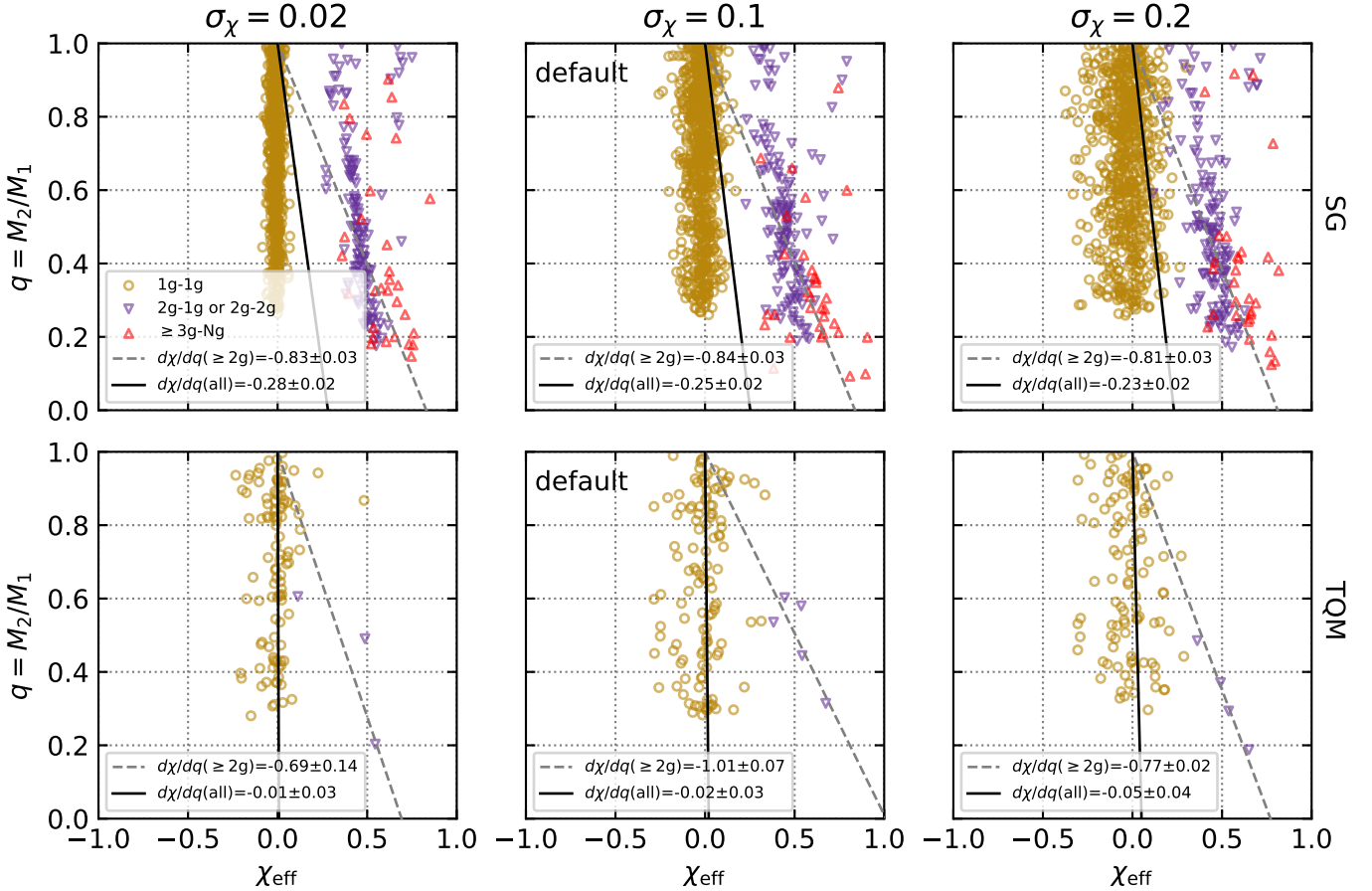


**Figure 4.** Varying the width of the Gaussian distribution for initial black hole spin magnitudes. *Top left:* SG disk with spin magnitude distribution  $\sigma_\chi = 0.02$ . *Top-center:* Default SG disk with  $\sigma_\chi = 0.1$ . *Top-right:* SG disk with  $\sigma_\chi = 0.2$ . *Bottom row:* Same as top row but for a TQM disk model. Narrower (wider) spin magnitude distributions primarily affect the 1g population by narrowing (widening) the distribution in  $\chi_{\text{eff}}$ . Markers are as in Fig. 1. See Table 1 for unique setup parameters and Table 2 for population statistics.

endfigure\*

Increasing  $f_{\text{ret}}$  to 0.5 continues this trend (top right, `sg_fr0p5`). The symmetry about  $\chi_{\text{eff}} = 0$  we have seen in the 1g population now extends to the hierarchical mergers. Since half of the hierarchical mergers now have  $\chi_{\text{eff}} < 0$ , the mean expectation value shifts to  $\overline{\chi_{\text{eff}}} = 0.01 \pm 0.45$ . There are no underlying differences to the hierarchical mergers compared to `sg_default` (top left), which can be seen by taking the absolute value of the effective spin before calculating the mean  $|\overline{\chi_{\text{eff}}}| = 0.45 \pm 0.09$  – consistent with  $\overline{\chi_{\text{eff}}} = 0.45 \pm 0.10$  seen in `sg_default`. Similar behavior is reflected in the  $\geq 3g$  population with  $\overline{\chi_{\text{eff}}} = 0.12 \pm 0.63$  vs.  $|\overline{\chi_{\text{eff}}}| = 0.62 \pm 0.14$  (see Table. 2).

The symmetry in the hierarchical population flattens the slopes of both line fits to  $d\chi_{\text{eff}}/dq = -0.04 \pm 0.02$  (all) and  $0.11 \pm 0.07$  ( $\geq 2g$ ). Retrograde binaries are not expected to form this frequently in an AGN disk, but

as one allows for more to occur, the number of negative  $\chi_{\text{eff}}$  events will increase, and the slopes flatten.

The bottom row of Fig. 5 shows the results for the TQM model. As opposed to the SG model, changing  $f_{\text{ret}}$  to 0.1 (bottom center, `tqm_fr0p1`) produces no  $\chi_{\text{eff}} < 0$  hierarchical mergers, but  $f_{\text{ret}} = 0.5$  (bottom right, `tqm_fr0p5`) does. There is no effect on the expectation values for the populations or slopes for the former case, but in the later case the hierarchical population is expected at  $\overline{\chi_{\text{eff}}} = -0.17 \pm 0.51$  and the overall fit is at  $d\chi_{\text{eff}}/dq = 0.07 \pm 0.04$ . However, this study is plagued by low number statistics from the inability of the TQM model to produce mergers from the default settings.

#### 4.8. Black Hole Orbital Eccentricity

In this section we explore the effects of changing the maximum initial orbital eccentricity of the embedded

## Retrograde Binary Fraction

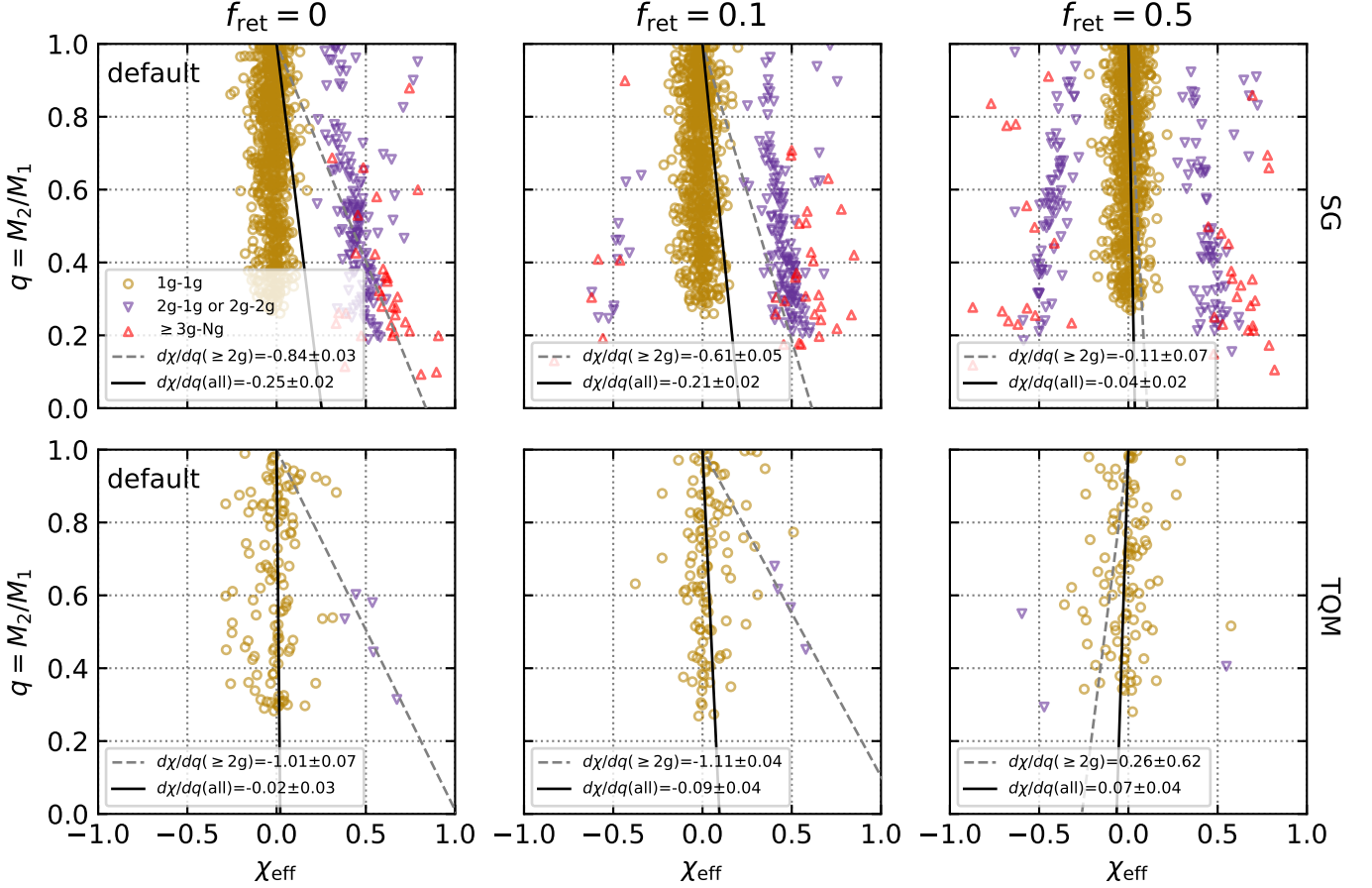


**Figure 5. Varying the retrograde binary fraction.** *Left column:* Default SG and TQM disk setups where no binaries allowed to form as retrograde ( $f_{\text{ret}} = 0$ ). *Center column:* Now the retrograde fraction is  $f_{\text{ret}} = 0.1$ . *Right column:* Half ( $f_{\text{ret}} = 0.5$ ) of binaries are allowed to form as retrograde. Increasing allowed retrograde fraction splits the hierarchical population to negative  $\chi_{\text{eff}}$  and flattens the slopes of the line fits for SG-like disks, but drawing conclusions in TQM-like disks is limit by low number statistics. Markers are as in Fig. 1. See Table 1 for unique setup parameters and Table 2 for population statistics.

black holes. Migration does not occur unless the black hole is on a relatively circular orbit, which we define as  $e_{\text{crit}} = 0.01$ . For eccentric prograde orbiters, mass accretion gradually causes the black hole spin to become anti-aligned to the disk. Thus, more eccentric orbits that spend a longer time circularizing experience more spin-down before they can migrate and form binaries.

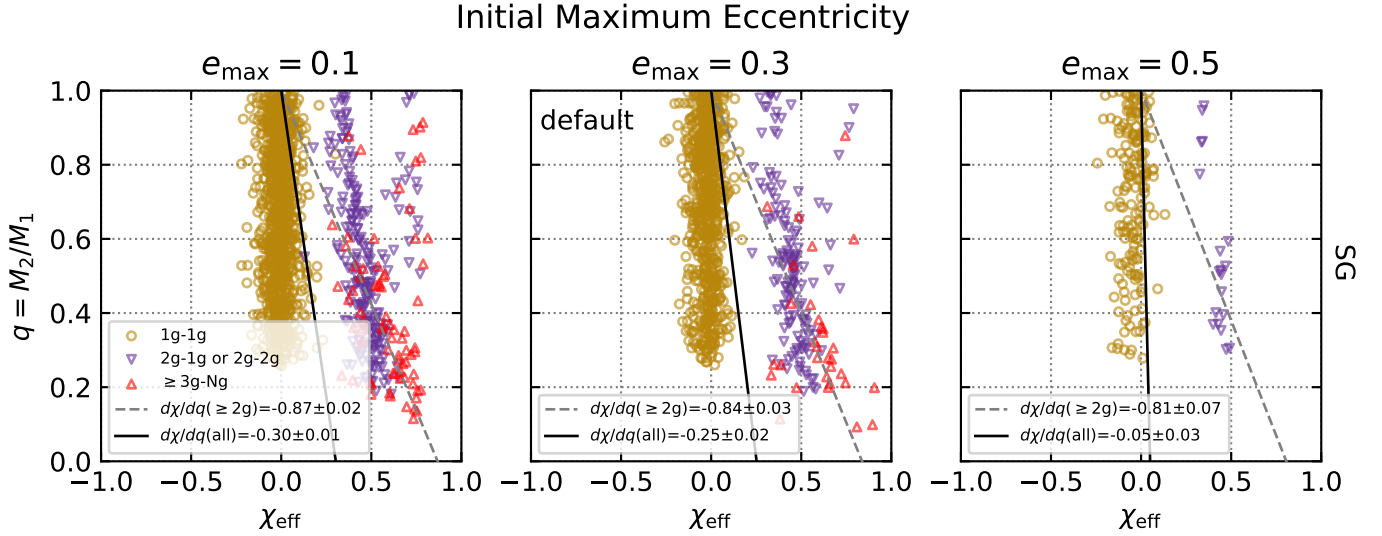
#### 4.8.1. SG disk: $e_{\text{max}} = 0.1, 0.3, 0.5$

Fig. 6 shows the results from a black hole population with orbits constrained to be more circular ( $e_{\text{max}} = 0.1$ , left panel, `sg_e0p1`) and relaxed to be more eccentric ( $e_{\text{max}} = 0.5$ , right panel, `sg_e0p5`). Starting from lower initial eccentricity, the 1g population becomes saturated across the entire range of possible mass ratios but no change occurs to the population's expectation values for  $q$  or  $\chi_{\text{eff}}$ . The same is true for the 2g and  $\geq 3g$  populations. The slope of the hierarchical fit does not

change from the default reflecting the similar expectation values, but the overall fit does slightly steepen from  $-0.25 \pm 0.01$  to  $-0.30 \pm 0.01$  due to the relative increase in number of hierarchical mergers. Conversely, the number of mergers decreases in each group from a more eccentric initial black holes population, and the suppression of hierarchical mergers flattens the overall line fit to a slope of  $-0.05 \pm 0.03$ .

Given a fixed disk lifetime, starting from a more circular population reduces time spent circularizing, jump starts the migration process, and increases the pool of black holes available to form binaries at early times. Since more black holes spend a longer time participating in mergers, the  $\geq 3g$  hierarchical merger population is able to reach lower mass ratios and higher effective spins.

#### 4.8.2. SG disk with thermal distribution: $e_{\text{max}} = 0.7$



**Figure 6. Varying the initial maximum orbital eccentricity.** SG disk with NSC initial eccentricity capped at  $e_{\max} = 0.1$  (left), 0.3 (default, center), and 0.5 (right). The number of mergers is inversely proportional to initial eccentricity. Markers are as in Fig. 1. See Table 1 for unique setup parameters and Table 2 for population statistics.

A thermal NSC is either one that has not had substantial activity or one that had sufficient time between active phases for dynamical encounters to erase the circularization caused by the accretion disk and as such has average orbital eccentricity of 0.7. Fig. 7 shows that a SG accretion disk interacting with this thermal black hole population for 0.75 Myr (center panel, `sg_e0p7`) suppresses almost all mergers. However, increasing the disk life time to 1.5 Myr (right panel, `sg_e0p7_t1p5`) provides sufficient time to damp this highly eccentric nuclear star cluster to broadly match the `sg_default` results. Though statistically the same, the 1g populations qualitatively shift towards negative  $\chi_{\text{eff}}$  (left panel:  $\overline{\chi_{\text{eff}}}(1g) = -0.01 \pm 0.11$ , right panel:  $-0.07 \pm 0.07$ ), since accretion-driven spin down during a lengthy circularization period leads to highly eccentric BHs entering a binary with spins pointing opposite to the binary orbital angular momentum.

Fundamentally, an accretion episode interacting with a thermal NSC requires a longer active state before mergers occur. Additionally, the 1g population will be slightly skewed towards negative  $\chi_{\text{eff}}$  values due to longer circularization timescales.

#### 4.8.3. TQM disk: $e_{\max} = 0.015, 0.05, 0.1$

The default TQM setup uses a lower eccentricity maximum  $e_{\max} = 0.05$  which we now vary to 0.015 and 0.1. Examining Fig. 8 shows that increasing the eccentricity to 0.1 (right panel, `tqm_e0p1`) leaves the hierarchical merger population unchanged and decreases the 1g merger population by roughly two thirds. Even this small eccentricity is enough to almost entirely suppress mergers. Conversely, when  $e_{\max} = 0.015$  (left

panel, `tqm_e0p015`), only 0.005 above our eccentricity criterion for treating orbits as circular, we see for the first time a distribution of 1g and hierarchical mergers that appears remotely similar to the SG model default from any parameter setup using the TQM model. The 1g population is densely concentrated about  $\chi_{\text{eff}} = 0$  with  $\overline{\chi_{\text{eff}}} = 0.03 \pm 0.09$  over the range of mass ratios  $0.25 \lesssim q \leq 1$  with  $\overline{q} = 0.69 \pm 0.21$ . The overall line fit is also the first produced by the TQM model to have non-zero slope and is similar to what was reported by Callister et al. (2021) at  $d\chi_{\text{eff}}/dq = -0.22 \pm 0.01$ . The hierarchical population is finally significant enough to do this with a slope fit of  $d\chi_{\text{eff}}/dq = -0.90 \pm 0.04$ , due to expectation values of  $\overline{\chi_{\text{eff}}} = 0.49 \pm 0.12$  and  $\overline{q} = 0.52 \pm 0.21$ .

#### 4.8.4. TQM disk with circular orbits: $e_{\max} = 0$

The TQM model has been unable to produce any significant number of hierarchical mergers with a slightly eccentric initial NSC. Here we explore how disk lifetime affects the  $q - \chi_{\text{eff}}$  plane, when the NSC starts from completely circular orbits.

Fig. 9 shows the results from evolving the circular NSC ( $e_{\max} = 0$ ) in a TQM disk for  $\tau_{\text{AGN}} = 1$  and 3 Myr compared with our default setup. The only difference between the 3 Myr run (center panel, `tqm_e0`) and the default setup (right panel) is the initial maximum eccentricity, but we can see the 1g and  $\geq 2g$  population islands have appeared mostly as seen in `sg_default` and `tqm_e0p015` models. The 1g population is still highly concentrated in effective spin expected at  $\overline{\chi_{\text{eff}}} = 0.03 \pm 0.09$  and mass ratio located around  $\overline{q} = 0.67 \pm 0.21$ . The 2g hierarchical population is similar to the SG default but the TQM model seems unable to

### Thermal Eccentricity Maximum: $e_{\max} = 0.7$

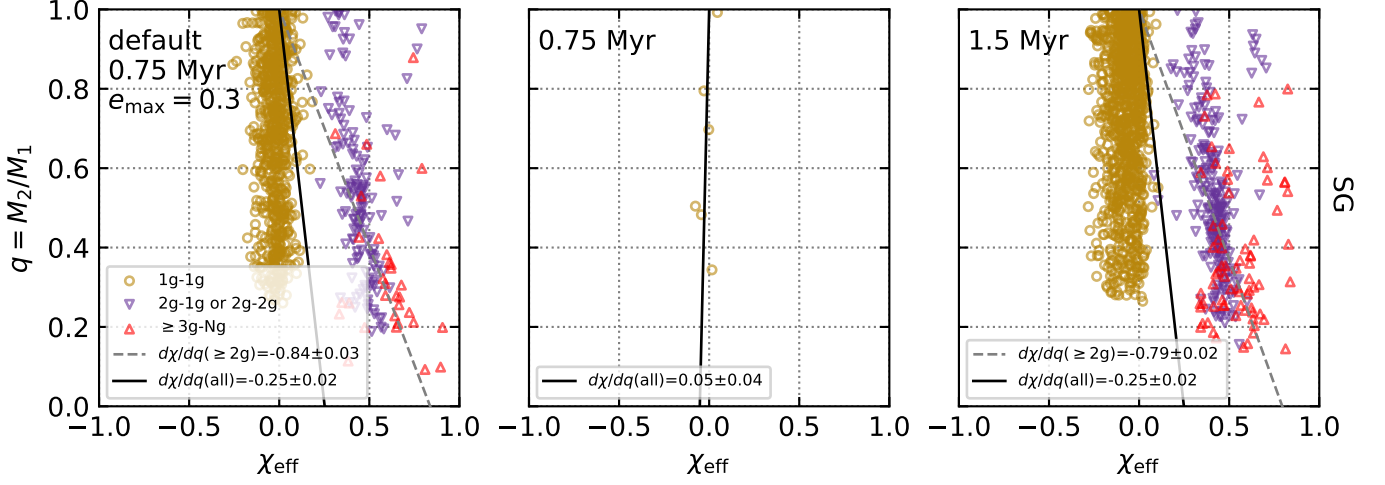


**Figure 7. Thermal Population with varying lifetimes.** *Left:* Default SG disk with  $e_{\max} = 0.3$ . *Center:* SG disk interacting with a thermal NSC with  $e_{\max} = 0.7$ . *Right:* Thermal NSC with SG disk lifetime increased to  $\tau_{\text{AGN}} = 1.5$  Myr. A more eccentric NSC takes longer to circularize which increases the time to produce mergers. Markers are as in Fig. 1. See Table 1 for unique setup parameters and Table 2 for population statistics.

### Initial Maximum Eccentricity

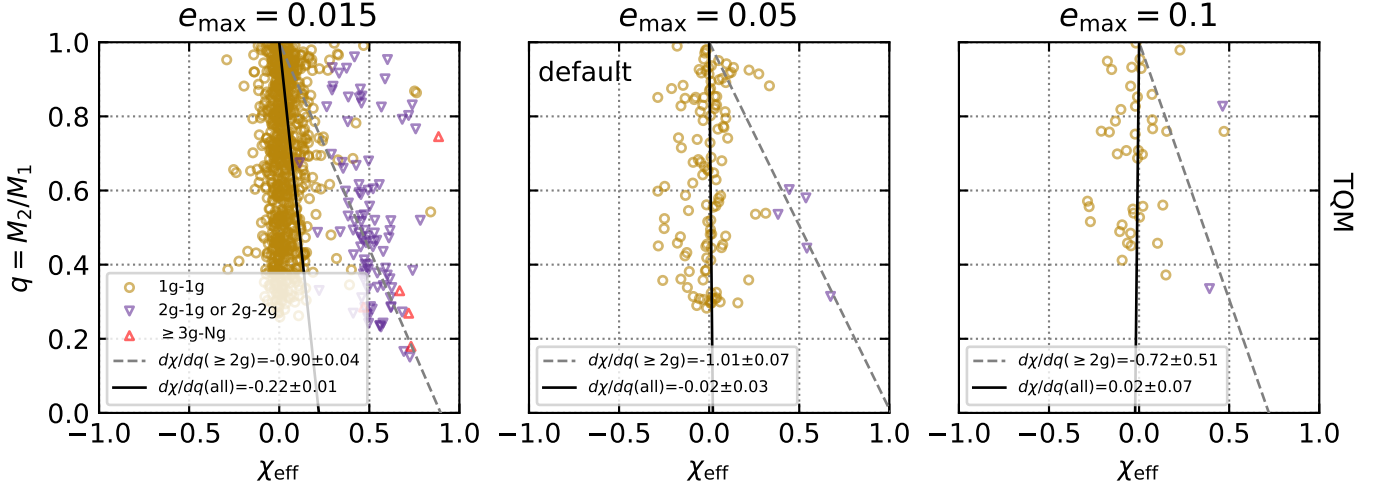


**Figure 8. Varying the initial maximum orbital eccentricity.** TQM disk with NSC initial eccentricity capped at  $e_{\max} = 0.015$  (left), 0.05 (default, center), and 0.1 (right). The number of mergers is inversely proportional to initial eccentricity, and an extremely low eccentricity is required for the TQM model to produce a distribution of mergers comparable to the SG model. Markers are as in Fig. 1. See Table 1 for unique setup parameters and Table 2 for population statistics.

produce extreme hierarchical mergers with only a handful of  $\geq 3g$  events. The mean effective spin for all hierarchical events is  $\overline{\chi_{\text{eff}}} = 0.50 \pm 0.12$ , and the mean mass ratio is  $\overline{q} = 0.53 \pm 0.21$ . Also of note, the slopes of the line fits have decreased. The hierarchical population fit is by a line with slope  $d\chi_{\text{eff}}/dq = -0.94 \pm 0.03$ , and the overall population is fit with a slope  $d\chi_{\text{eff}}/dq = -0.21 \pm 0.01$ . This is the second test in a TQM disk with a slope similar to that reported by Callister et al. (2021) for the LVK observations to-date.

The left panel of Fig. 9 shows a run with the same setup using a different random seed but only ran for 1 Myr ( $\tau_{\text{qm\_e0\_t1}}$ ). The populations look very similar to the 3 Myr run with not much decrease in the number of hierarchical mergers despite the shorter evolution time, and some high generation ( $\geq 3g$ ) black holes still participate in mergers. After 1 Myr, the expectation values for all populations and slopes are statistically identical to the 3 Myr run.

By skipping the damping process for eccentric orbits, a circular population of black holes interacting within a TQM-like disk can immediately migrate, form binaries, and merge. By jump-starting the merger process, hierarchical mergers occur readily within 1 Myr. However, far fewer higher generation ( $\geq 3g$ ) mergers occur compared to SG. This behavior suggests TQM-like disks quickly exhaust the embedded 1g population, and are unable to continue merging higher generation binaries, because of slow (inefficient) migration. Thus, low density disks with dynamically cooled populations could contribute to the 1g population without significantly contributing to high mass BBH mergers.

## 5. DISCUSSION

One of the most intriguing results to emerge from the LVK O3 GW results was an apparent anti-correlation between BBH mass ratio ( $q = M_2/M_1$ ) and the BBH effective spin ( $\chi_{\text{eff}}$ ) (Callister et al. 2021). At first glance this seems unexpected from most channels. The AGN channel was recognized as a possible source of such an anti-correlation simply because: a) more massive black hole ( $M_1$ ) should spend longer in AGN disks and so, b) primary black hole ( $M_1$ ) spins should be biased towards alignment with the orbital angular momentum of the disk (and the BBH) (e.g. McKernan et al. 2022a; Santini et al. 2023; Dittmann et al. 2024). Here we have demonstrated the form of the  $q - \chi_{\text{eff}}$  parameter space distribution as a function of different disk and model choices for the AGN channel.

First, and most importantly, our default choice of a SG disk run for 1 Myr with a  $\gamma = 2$  IMF seems to be a reasonable fit to the observed  $q - \chi_{\text{eff}}$  distribution (see Fig. 1 top left panel). Callister et al. (2021) find an overall anti-correlation fit of  $d\chi_{\text{eff}}/dq \sim -0.46_{-0.28}^{+0.29}$  for their distribution when they exclude GW190814. However, when they include GW190814, they find  $d\chi_{\text{eff}}/dq = -0.28_{-0.28}^{+0.31}$  which is very similar to our  $d\chi_{\text{eff}}/dq = -0.25 \pm 0.02$  from our default SG model. This highlights an important point: GW190814 is difficult to reproduce commonly in any other channel, however in AGN (depending on choice of IMF) such low  $q \sim 0.1$  events can occur at the few percent level (Secunda et al. 2019; McKernan et al. 2020a; Tagawa et al. 2020b).

Second, it is clear that the AGN channel produces islands of population in  $q - \chi_{\text{eff}}$  parameter space. Evidently the 1g mergers tend (at least in dense SG-like disks) to be concentrated around  $\chi_{\text{eff}} \sim 0$ . Higher generation hierarchical mergers ( $\geq 2g$ ) tend to live in islands at higher  $\chi_{\text{eff}}$ . Indeed the structure, location and density of these population islands is what drives the  $d\chi_{\text{eff}}/dq$  in the AGN channel. For example, a steep IMF ( $\gamma = 2$ )

tends to drive  $q \sim 0.7$  mergers, whereas a flatter IMF ( $\gamma = 1$ ) drives lower  $q$  mergers and drives the average ( $d\chi_{\text{eff}}/dq$ ) slope to more negative values (compare Fig. 1 top panels). Future LVK results (e.g. from O4) can constrain the presence (or not) of such islands.

Third, while higher-density SG disks can reproduce the  $d\chi_{\text{eff}}/dq$  correlation, we find that low-density AGN disk models can only reproduce this correlation if the initial black hole population has been dynamically cooled (compare e.g. Fig. 1 bottom panels and Fig. 9). Indeed some level of dynamical cooling is also preferred in denser SG-like disks (see Fig. 6). Only very small initial eccentricities for black holes embedded in TQM-like disk models can reproduce the observed  $d\chi_{\text{eff}}/dq$  anti-correlation (Callister et al. 2021). Lower surface density disk models like TQM take longer to circularize and migrate embedded black holes, leading to low merger rates than SG-like models. If we extend the disk lifetime ( $\tau_{\text{AGN}}$ ), we can drive a higher BBH merger rate, but at the expense of spin down due to retrograde accretion from the gas disk for an initially eccentric population (see Fig. 2 bottom panels). So it is unlikely that low density disks are a significant contributor to the observed LVK rate among higher mass mergers unless their initial populations are dynamically cold (low  $e$ ).

Fourth, as the width of black holes' initial spin distribution  $\sigma_\chi$  increases, the width of the islands in  $q - \chi_{\text{eff}}$  parameter space increases (see gold, purple and red populations in Fig. 4). Larger values of  $\sigma_\chi$  lead to a larger weighting of the 1g population to negative  $\chi_{\text{eff}}$ . We constrain  $\sigma_\chi \leq 0.2$  in the AGN channel from LVK observations.

Fifth, the gradient ( $d\chi_{\text{eff}}/dq$ ) in the AGN channel is also driven by the ratio ( $f_{\text{ret}}$ ) of retrograde/prograde BBH mergers. For  $f_{\text{ret}} = [0, 0.1, 5]$ , the gradient  $d\chi_{\text{eff}}/dq = [-0.25 \pm 0.02, -0.21 \pm 0.02, -0.04 \pm 0.02]$  for our default model in an SG disk. As Callister et al. (2021) find  $d\chi_{\text{eff}}/dq = -0.28_{-0.28}^{+0.31}$  from O3, a low value of  $f_{\text{ret}}$  is preferred, but we cannot exclude  $f_{\text{ret}} \sim 0.5$ . The value of  $f_{\text{ret}}$  for mergers in AGN disks remains an unsolved problem. The change in separation between BBH formation and merger is 6-7 orders of magnitude and the details of what happens during hardening in AGN remain unclear. BBH formation via GW capture in gas disks can be either prograde or retrograde (e.g. DeLaurentiis et al. 2023; Whitehead et al. 2024; Qian et al. 2024). However, retrograde BBH may have their eccentricity pumped (Li & Lai 2022; Calcino et al. 2023), and may therefore harden quickly towards merger. However, there is much debate as to whether retrograde BBH are preferentially ionized as their eccentricity is pumped (Wang et al. 2021), or whether they are flipped to pro-

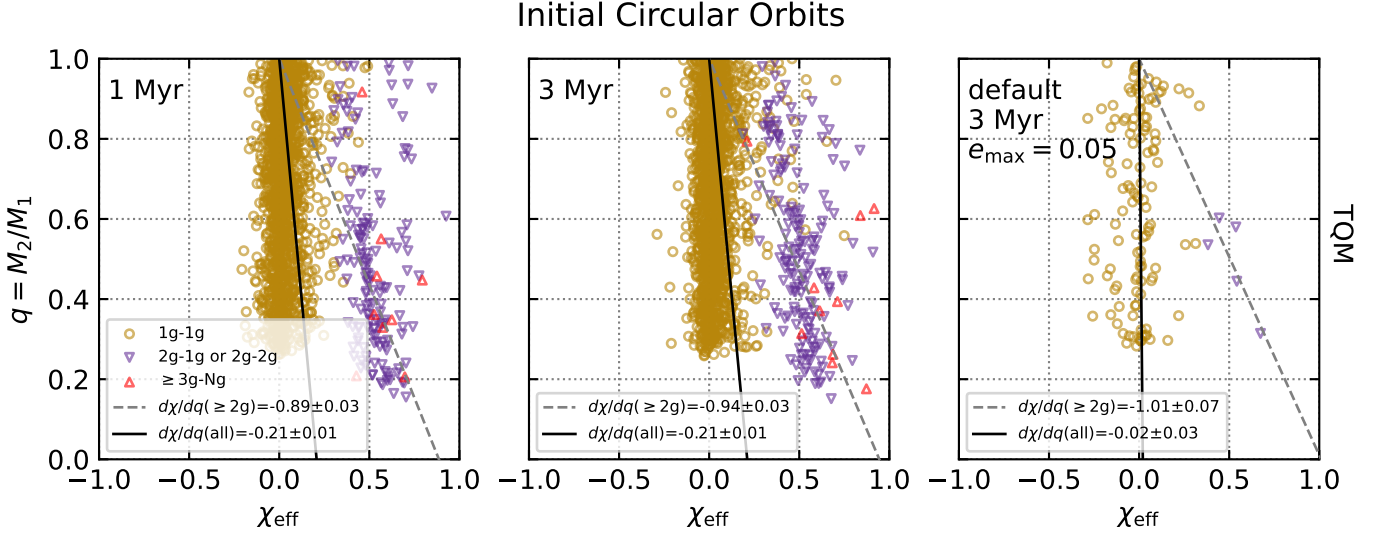


**Figure 9. Initially circular orbits with varying AGN lifetimes.** *Left:* TQM disk with black holes on initially circular orbits evolved for  $\tau_{\text{AGN}} = 1$  Myr. *Center:* Setup same as the TQM default but with circular black hole orbits ( $\tau_{\text{AGN}} = 3$  Myr). *Right:* Default TQM setup where  $\tau_{\text{AGN}} = 3$  Myr and initial eccentricity is capped at  $e_{\text{max}} = 0.05$ . Markers are as in Fig. 1. See Table 1 for unique setup parameters and Table 2 for population statistics.

grade due to dynamical encounters (Samsing et al. 2022; McKernan & Ford 2024). The slope of the ( $d\chi_{\text{eff}}/dq$ ) anti-correlation that emerges from larger data sets (O4, O5) will allow us to directly test models of the retrograde fraction of BBH in the AGN channel.

Sixth, disk size impacts both the overall rate of BBH mergers and the  $q - \chi_{\text{eff}}$  distribution (see Fig. 3). A small average disk size generates a plausible  $q - \chi_{\text{eff}}$  distribution but a far lower merger rate. Extending the disk into a less dense NSC and then assuming a uniform distribution of black holes (our default model) also lowers the merger rate. In the future, modifying the black hole distribution so that it matches the black hole density distribution of the NSC will enhance the importance of the inner disk for mergers.

## 6. CONCLUSION

We use the new public, open-source, reproducible code McFACTS to test the  $q - \chi_{\text{eff}}$  distribution for the LVK AGN channel. Broadly we find islands of structure in  $q - \chi_{\text{eff}}$  parameter space as a function of black hole generation, spin and eccentricity distributions and disk models and duration. The observed  $q - \chi_{\text{eff}}$  anti-correlation is well reproduced by a dense and relatively short-lived

model AGN disk with some dynamical cooling. Tighter constraints on the  $q - \chi_{\text{eff}}$  distribution from future LVK BBH catalogs (O4 and O5) will allow us to strongly constrain key AGN disk and NSC properties.

HEC, BM & KESF are supported by NSF AST-2206096. BM & KESF are also supported by Simons Foundation Grant 533845 as well as Simons Foundation sabbatical support. The Flatiron Institute is supported by the Simons Foundation. ROS gratefully acknowledges support from NSF awards NSF PHY-1912632, PHY-2012057, PHY-2309172, AST-2206321, and the Simons Foundation. VD is supported by an appointment to the NASA Postdoctoral Program at the NASA Goddard Space Flight Center administered by Oak Ridge Associated Universities under contract NPP-GSFC-NOV21-0031. KN thanks the LSST-DA Data Science Fellowship Program, which is funded by LSST-DA, the Brinson Foundation, and the Moore Foundation; her participation in the program has benefited this work.

*Software:* Astropy, (Astropy Collaboration et al. 2013, 2018), pAGN (Gangardt et al. 2024b), NumPy (Harris et al. 2020), SciPy (Virtanen et al. 2020), Matplotlib (Hunter 2007).

## REFERENCES

Antonini, F., & Rasio, F. A. 2016, ApJ, 831, 187,

doi: 10.3847/0004-637X/831/2/187

Arca Sedda, M., Naoz, S., & Kocsis, B. 2023, Universe, 9,

138, doi: 10.3390/universe9030138

- Astropy Collaboration, Robitaille, T. P., Tollerud, E. J., et al. 2013, *A&A*, 558, A33, doi: [10.1051/0004-6361/201322068](https://doi.org/10.1051/0004-6361/201322068)
- Astropy Collaboration, Price-Whelan, A. M., Sipőcz, B. M., et al. 2018, *AJ*, 156, 123, doi: [10.3847/1538-3881/aabc4f](https://doi.org/10.3847/1538-3881/aabc4f)
- Bartos, I., Kocsis, B., Haiman, Z., & Márka, S. 2017, *ApJ*, 835, 165, doi: [10.3847/1538-4357/835/2/165](https://doi.org/10.3847/1538-4357/835/2/165)
- Belczynski, K., Heger, A., Gladysz, W., et al. 2016, *A&A*, 594, A97, doi: [10.1051/0004-6361/201628980](https://doi.org/10.1051/0004-6361/201628980)
- Bellovary, J. M., Mac Low, M.-M., McKernan, B., & Ford, K. E. S. 2016, *ApJL*, 819, L17, doi: [10.3847/2041-8205/819/2/L17](https://doi.org/10.3847/2041-8205/819/2/L17)
- Calcino, J., Dempsey, A. M., Dittmann, A. J., & Li, H. 2023, arXiv e-prints, arXiv:2311.13727, doi: [10.48550/arXiv.2311.13727](https://doi.org/10.48550/arXiv.2311.13727)
- Callister, T. A. 2021, arXiv e-prints, arXiv:2104.09508, doi: [10.48550/arXiv.2104.09508](https://doi.org/10.48550/arXiv.2104.09508)
- Callister, T. A., Haster, C.-J., Ng, K. K. Y., Vitale, S., & Farr, W. M. 2021, *ApJL*, 922, L5, doi: [10.3847/2041-8213/ac2ccc](https://doi.org/10.3847/2041-8213/ac2ccc)
- DeLaurentiis, S., Epstein-Martin, M., & Haiman, Z. 2023, *MNRAS*, 523, 1126, doi: [10.1093/mnras/stad1412](https://doi.org/10.1093/mnras/stad1412)
- Delfavero, V., Ford, K. E. S., McKernan, B., et al. 2024, arXiv e-prints, arXiv:2410.18815, doi: [10.48550/arXiv.2410.18815](https://doi.org/10.48550/arXiv.2410.18815)
- Dittmann, A. J., Dempsey, A. M., & Li, H. 2024, *ApJ*, 964, 61, doi: [10.3847/1538-4357/ad23ce](https://doi.org/10.3847/1538-4357/ad23ce)
- Dodici, M., & Tremaine, S. 2024, arXiv e-prints, arXiv:2404.08138, doi: [10.48550/arXiv.2404.08138](https://doi.org/10.48550/arXiv.2404.08138)
- Fabj, G., Nasim, S. S., Caban, F., et al. 2020, *MNRAS*, 499, 2608, doi: [10.1093/mnras/staa3004](https://doi.org/10.1093/mnras/staa3004)
- Ford, K. E. S., & McKernan, B. 2022, *MNRAS*, 517, 5827, doi: [10.1093/mnras/stac2861](https://doi.org/10.1093/mnras/stac2861)
- Gangardt, D., Trani, A. A., Bonnerot, C., & Gerosa, D. 2024a, *MNRAS*, 530, 3689, doi: [10.1093/mnras/stae1117](https://doi.org/10.1093/mnras/stae1117)
- . 2024b, *MNRAS*, 530, 3689, doi: [10.1093/mnras/stae1117](https://doi.org/10.1093/mnras/stae1117)
- Generozov, A., Stone, N. C., Metzger, B. D., & Ostriker, J. P. 2018, *MNRAS*, 478, 4030, doi: [10.1093/mnras/sty1262](https://doi.org/10.1093/mnras/sty1262)
- Harris, C. R., Millman, K. J., van der Walt, S. J., et al. 2020, *Nature*, 585, 357, doi: [10.1038/s41586-020-2649-2](https://doi.org/10.1038/s41586-020-2649-2)
- Hunter, J. D. 2007, *Computing in Science & Engineering*, 9, 90, doi: [10.1109/MCSE.2007.55](https://doi.org/10.1109/MCSE.2007.55)
- Li, R., & Lai, D. 2022, *MNRAS*, 517, 1602, doi: [10.1093/mnras/stac2577](https://doi.org/10.1093/mnras/stac2577)
- Lu, J. R., Do, T., Ghez, A. M., et al. 2013, *ApJ*, 764, 155, doi: [10.1088/0004-637X/764/2/155](https://doi.org/10.1088/0004-637X/764/2/155)
- Lyra, W., Paardekooper, S.-J., & Mac Low, M.-M. 2010, *ApJL*, 715, L68, doi: [10.1088/2041-8205/715/2/L68](https://doi.org/10.1088/2041-8205/715/2/L68)
- McKernan, B., & Ford, K. E. S. 2024, *MNRAS*, 531, 3479, doi: [10.1093/mnras/stae1351](https://doi.org/10.1093/mnras/stae1351)
- McKernan, B., Ford, K. E. S., Callister, T., et al. 2022a, *MNRAS*, 514, 3886, doi: [10.1093/mnras/stac1570](https://doi.org/10.1093/mnras/stac1570)
- McKernan, B., Ford, K. E. S., Cantiello, M., et al. 2022b, *MNRAS*, 514, 4102, doi: [10.1093/mnras/stac1310](https://doi.org/10.1093/mnras/stac1310)
- McKernan, B., Ford, K. E. S., Cook, H. E., et al. 2024, arXiv e-prints, arXiv:2410.16515, doi: [10.48550/arXiv.2410.16515](https://doi.org/10.48550/arXiv.2410.16515)
- McKernan, B., Ford, K. E. S., Kocsis, B., Lyra, W., & Winter, L. M. 2014, *MNRAS*, 441, 900, doi: [10.1093/mnras/stu553](https://doi.org/10.1093/mnras/stu553)
- McKernan, B., Ford, K. E. S., Lyra, W., & Perets, H. B. 2012, *MNRAS*, 425, 460, doi: [10.1111/j.1365-2966.2012.21486.x](https://doi.org/10.1111/j.1365-2966.2012.21486.x)
- McKernan, B., Ford, K. E. S., & O’Shaughnessy, R. 2020a, *MNRAS*, 498, 4088, doi: [10.1093/mnras/staa2681](https://doi.org/10.1093/mnras/staa2681)
- McKernan, B., Ford, K. E. S., O’Shaughnessy, R., & Wysocki, D. 2020b, *MNRAS*, 494, 1203, doi: [10.1093/mnras/staa740](https://doi.org/10.1093/mnras/staa740)
- Nasim, S. S., Fabj, G., Caban, F., et al. 2023, *MNRAS*, 522, 5393, doi: [10.1093/mnras/stad1295](https://doi.org/10.1093/mnras/stad1295)
- Qian, K., Li, J., & Lai, D. 2024, *ApJ*, 962, 143, doi: [10.3847/1538-4357/ad1b53](https://doi.org/10.3847/1538-4357/ad1b53)
- Renzo, M., & Smith, N. 2024, arXiv e-prints, arXiv:2407.16113, doi: [10.48550/arXiv.2407.16113](https://doi.org/10.48550/arXiv.2407.16113)
- Rodriguez, C. L., Amaro-Seoane, P., Chatterjee, S., & Rasio, F. A. 2018, *PhRvL*, 120, 151101, doi: [10.1103/PhysRevLett.120.151101](https://doi.org/10.1103/PhysRevLett.120.151101)
- Rowan, C., Boeholt, T., Kocsis, B., & Haiman, Z. 2023, *MNRAS*, 524, 2770, doi: [10.1093/mnras/stad1926](https://doi.org/10.1093/mnras/stad1926)
- Samsing, J., Bartos, I., D’Orazio, D. J., et al. 2022, *Nature*, 603, 237, doi: [10.1038/s41586-021-04333-1](https://doi.org/10.1038/s41586-021-04333-1)
- Santini, A., Gerosa, D., Cotesta, R., & Berti, E. 2023, arXiv e-prints, arXiv:2308.12998, doi: [10.48550/arXiv.2308.12998](https://doi.org/10.48550/arXiv.2308.12998)
- Secunda, A., Bellovary, J., Mac Low, M.-M., et al. 2019, *ApJ*, 878, 85, doi: [10.3847/1538-4357/ab20ca](https://doi.org/10.3847/1538-4357/ab20ca)
- Secunda, A., Hernandez, B., Goodman, J., et al. 2021, *ApJL*, 908, L27, doi: [10.3847/2041-8213/abe11d](https://doi.org/10.3847/2041-8213/abe11d)
- Sirko, E., & Goodman, J. 2003, *MNRAS*, 341, 501, doi: [10.1046/j.1365-8711.2003.06431.x](https://doi.org/10.1046/j.1365-8711.2003.06431.x)
- Stone, N. C., Metzger, B. D., & Haiman, Z. 2017, *MNRAS*, 464, 946, doi: [10.1093/mnras/stw2260](https://doi.org/10.1093/mnras/stw2260)
- Tagawa, H., Haiman, Z., Bartos, I., & Kocsis, B. 2020a, *ApJ*, 899, 26, doi: [10.3847/1538-4357/aba2cc](https://doi.org/10.3847/1538-4357/aba2cc)
- Tagawa, H., Haiman, Z., & Kocsis, B. 2020b, *ApJ*, 898, 25, doi: [10.3847/1538-4357/ab9b8c](https://doi.org/10.3847/1538-4357/ab9b8c)

- The LIGO Scientific Collaboration, the Virgo Collaboration, the KAGRA Collaboration, & Abbott, R. e. a. 2021, arXiv e-prints, arXiv:2111.03606, doi: [10.48550/arXiv.2111.03606](https://doi.org/10.48550/arXiv.2111.03606)
- Thompson, T. A., Quataert, E., & Murray, N. 2005, *ApJ*, 630, 167, doi: [10.1086/431923](https://doi.org/10.1086/431923)
- Tichy, W., & Marronetti, P. 2008, *PhRvD*, 78, 081501, doi: [10.1103/PhysRevD.78.081501](https://doi.org/10.1103/PhysRevD.78.081501)
- Vaccaro, M. P., Mapelli, M., Périgois, C., et al. 2024, *A&A*, 685, A51, doi: [10.1051/0004-6361/202348509](https://doi.org/10.1051/0004-6361/202348509)
- Vajpeyi, A., Thrane, E., Smith, R., McKernan, B., & Saavik Ford, K. E. 2022, *ApJ*, 931, 82, doi: [10.3847/1538-4357/ac6180](https://doi.org/10.3847/1538-4357/ac6180)
- Virtanen, P., Gommers, R., Oliphant, T. E., et al. 2020, *Nature Methods*, 17, 261, doi: [10.1038/s41592-019-0686-2](https://doi.org/10.1038/s41592-019-0686-2)
- Wang, Y., Zhu, Z., & Lin, D. N. C. 2024, *MNRAS*, 528, 4958, doi: [10.1093/mnras/stae321](https://doi.org/10.1093/mnras/stae321)
- Wang, Y.-H., McKernan, B., Ford, S., et al. 2021, *ApJL*, 923, L23, doi: [10.3847/2041-8213/ac400a](https://doi.org/10.3847/2041-8213/ac400a)
- Whitehead, H., Rowan, C., Boehholt, T., & Kocsis, B. 2024, *MNRAS*, 531, 4656, doi: [10.1093/mnras/stae1430](https://doi.org/10.1093/mnras/stae1430)
- Yang, Y., Bartos, I., Gayathri, V., et al. 2019, *PhRvL*, 123, 181101, doi: [10.1103/PhysRevLett.123.181101](https://doi.org/10.1103/PhysRevLett.123.181101)

Table 2. Statistical estimates of the merger events.

Run	Fig.	$d\chi_{\text{eff}}/dq$				1g-1g				$\geq 2g$ -Ng				$\geq 3g$ -Ng			
		all	$\geq 2g$	N	$\bar{q}$	$\overline{\chi_{\text{eff}}}$	N	$\bar{q}$	$\overline{\chi_{\text{eff}}}$	N	$\bar{q}$	$\overline{\chi_{\text{eff}}}$	N	$\bar{q}$	$\overline{\chi_{\text{eff}}}$		
sg_default	1	-0.25 ± 0.02	-0.84 ± 0.03	712	0.69 ± 0.21	-0.02 ± 0.06	138	0.54 ± 0.21	0.45 ± 0.10	32	0.34 ± 0.18	0.60 ± 0.15					
tqm_default	1	-0.02 ± 0.03	-1.01 ± 0.07	119	0.64 ± 0.22	-0.01 ± 0.11	5	0.50 ± 0.11	0.52 ± 0.10	0	—	—					
sg-g1	1	-0.31 ± 0.01	-0.82 ± 0.02	1047	0.66 ± 0.21	-0.02 ± 0.06	257	0.52 ± 0.23	0.45 ± 0.11	84	0.35 ± 0.19	0.59 ± 0.15					
tqm-g1	1	0.01 ± 0.03	-0.51 ± 0.05	131	0.67 ± 0.22	-0.03 ± 0.12	2	0.26 ± 0.01	0.37 ± 0.04	0	—	—					
sg-t0p5	2	-0.08 ± 0.02	-0.83 ± 0.06	199	0.69 ± 0.20	-0.02 ± 0.05	17	0.56 ± 0.22	0.42 ± 0.08	1	0.18 ± 0.00	0.69 ± 0.00					
sg-t5	2	-0.34 ± 0.01	-0.83 ± 0.02	1080	0.70 ± 0.21	-0.02 ± 0.06	266	0.53 ± 0.21	0.45 ± 0.10	105	0.38 ± 0.21	0.57 ± 0.15					
tqm-t2p5	2	-0.11 ± 0.03	-0.75 ± 0.09	107	0.69 ± 0.21	0.01 ± 0.08	7	0.50 ± 0.18	0.43 ± 0.10	1	0.30 ± 0.00	0.45 ± 0.00					
tqm-t5	2	0.11 ± 0.04	-0.65 ± 0.24	116	0.64 ± 0.21	-0.05 ± 0.15	3	0.61 ± 0.15	0.30 ± 0.06	0	—	—					
sg-r2e4	3	-0.27 ± 0.04	-0.83 ± 0.06	69	0.66 ± 0.19	0.02 ± 0.07	9	0.49 ± 0.16	0.43 ± 0.08	3	0.29 ± 0.15	0.67 ± 0.04					
sg-r1e5	3	-0.08 ± 0.05	-0.87 ± 0.13	50	0.69 ± 0.22	-0.03 ± 0.08	4	0.54 ± 0.18	0.45 ± 0.06	0	—	—					
tqm-r2e4	3	—	—	0	—	—	0	—	—	0	—	—					
tqm-r1e5	3	-0.15 ± 0.02	-0.83 ± 0.06	179	0.67 ± 0.22	0.05 ± 0.10	4	0.39 ± 0.16	0.51 ± 0.09	0	—	—					
sg-s0p02	4	-0.28 ± 0.02	-0.83 ± 0.03	682	0.70 ± 0.20	-0.01 ± 0.02	131	0.52 ± 0.22	0.46 ± 0.09	30	0.42 ± 0.23	0.59 ± 0.13					
sg-s0p20	4	-0.23 ± 0.02	-0.81 ± 0.03	708	0.68 ± 0.20	-0.03 ± 0.10	135	0.50 ± 0.22	0.44 ± 0.10	30	0.38 ± 0.21	0.62 ± 0.12					
tqm-s0p02	4	-0.01 ± 0.03	-0.69 ± 0.14	106	0.69 ± 0.21	-0.01 ± 0.09	3	0.43 ± 0.17	0.38 ± 0.19	0	—	—					
tqm-s0p20	4	-0.05 ± 0.04	-0.77 ± 0.02	106	0.67 ± 0.21	-0.03 ± 0.13	4	0.33 ± 0.11	0.51 ± 0.10	0	—	—					
sg-fr0p1	5	-0.21 ± 0.02	-0.61 ± 0.05	729	0.68 ± 0.20	-0.01 ± 0.06	142	0.47 ± 0.19	0.38 ± 0.28	32	0.37 ± 0.18	0.38 ± 0.48					
sg-fr0p5	5	-0.04 ± 0.02	-0.11 ± 0.07	702	0.70 ± 0.20	0.00 ± 0.06	137	0.54 ± 0.22	0.01 ± 0.45	36	0.39 ± 0.22	0.12 ± 0.63					
tqm-fr0p1	5	-0.09 ± 0.04	-1.11 ± 0.04	108	0.68 ± 0.20	0.03 ± 0.12	4	0.58 ± 0.08	0.47 ± 0.07	0	—	—					
tqm-fr0p5	5	0.07 ± 0.04	0.26 ± 0.62	99	0.66 ± 0.20	-0.02 ± 0.13	3	0.42 ± 0.10	-0.17 ± 0.51	0	—	—					
sg-e0p1	6	-0.30 ± 0.01	-0.87 ± 0.02	1057	0.68 ± 0.20	-0.01 ± 0.06	223	0.54 ± 0.21	0.47 ± 0.11	73	0.41 ± 0.21	0.60 ± 0.14					
sg-e0p5	6	-0.05 ± 0.03	-0.81 ± 0.07	177	0.72 ± 0.20	-0.05 ± 0.06	19	0.56 ± 0.21	0.42 ± 0.05	0	—	—					
sg-e0p7	7	—	—	6	0.64 ± 0.22	-0.01 ± 0.04	0	—	—	0	—	—					
sg-e0p7_t1p5	7	-0.25 ± 0.02	-0.79 ± 0.02	970	0.72 ± 0.20	-0.07 ± 0.07	224	0.54 ± 0.19	0.41 ± 0.09	73	0.38 ± 0.17	0.55 ± 0.14					
tqm-e0p015	8	-0.22 ± 0.01	-0.90 ± 0.04	867	0.69 ± 0.21	0.03 ± 0.09	96	0.52 ± 0.21	0.49 ± 0.12	5	0.36 ± 0.20	0.69 ± 0.13					
tqm-e0p1	8	0.02 ± 0.07	-0.72 ± 0.51	41	0.70 ± 0.18	-0.03 ± 0.14	2	0.58 ± 0.25	0.43 ± 0.04	0	—	—					
tqm-e0.t1	9	-0.21 ± 0.01	-0.89 ± 0.03	1586	0.68 ± 0.20	0.03 ± 0.08	152	0.50 ± 0.23	0.52 ± 0.12	9	0.43 ± 0.20	0.58 ± 0.11					
tqm-e0	9	-0.21 ± 0.01	-0.94 ± 0.03	1604	0.67 ± 0.21	0.03 ± 0.09	171	0.53 ± 0.21	0.50 ± 0.12	10	0.42 ± 0.19	0.66 ± 0.19					

NOTE—We report the  $d\chi_{\text{eff}}/dq$  slopes of lines fit to all mergers and the hierarchical sub-population ( $\geq 2g$ ) anchored through the point  $(\chi_{\text{eff}}, q) = (0, 1)$ , the number of mergers, the mean mass ratio  $\bar{q}$ , mean effective spin  $\overline{\chi_{\text{eff}}}$ , and relevant standard deviations, for 1g-1g,  $\geq 2g$ -Ng, and  $\geq 3g$ -Ng merger events in the associated figure.